PDGFR dimer-specific activation, trafficking and downstream signaling dynamics

Madison A. Rogers, Maria B. Campaña, Robert Long and Katherine A. Fantauzzo*

Department of Craniofacial Biology, School of Dental Medicine, University of Colorado Anschutz Medical Campus, Aurora, CO

*Author for correspondence (katherine.fantauzzo@cuanschutz.edu)

Keywords: PDGFRα, PDGFRβ, trafficking, signaling, proliferation, migration

Summary statement

A novel bimolecular fluorescence complementation approach reveals differences in the timing and extent of PDGFRα versus PDGFRβ homodimer activation, trafficking and downstream signaling.

Abstract

Signaling through the platelet-derived growth factor receptors (PDGFRs) plays a critical role in multiple cellular processes during development. The two PDGFRs, PDGFRα and PDGFRβ, dimerize to form homodimers and/or heterodimers. Here, we overcome previous limitations in studying PDGFR dimer-specific dynamics by generating cell lines stably expressing C-terminal fusions of each PDGFR with bimolecular fluorescence complementation (BiFC) fragments corresponding to the N-terminal or C-terminal regions of the Venus fluorescent protein. We find that PDGFRβ receptors homodimerize more quickly than PDGFRα receptors in response to PDGF ligand, with increased levels of autophosphorylation. Further, we demonstrate that PDGFRα homodimers are trafficked and degraded more quickly, while PDGFRβ homodimers are more likely to be recycled back to the cell membrane. We show that PDGFRβ homodimer activation results in a greater amplitude of phospho-ERK1/2 and phospho-AKT signaling, as well as increased proliferation and migration. Finally, we demonstrate that inhibition of clathrin-

mediated endocytosis leads to changes in cellular trafficking and downstream signaling, particularly for PDGFRα homodimers. Collectively, our findings provide significant insight into how biological specificity is introduced to generate unique responses downstream of PDGFR engagement.

Introduction

The platelet-derived growth factor receptors (PDGFRs) are a family of receptor tyrosine kinases (RTKs) known to direct multiple cellular processes during development, such as migration, proliferation and differentiation (Heldin and Westermark, 1999; Hoch and Soriano, 2003). In mammals, this family is composed of four dimeric growth factor ligands – PDGF-AA, PDGF-BB, PDGF-CC and PDGF-DD – which variously signal through two receptors, PDGFRα and PDGFRβ (Bostrom et al., 1996; Ding et al., 2004; Leveen et al., 1994; Soriano, 1994; Soriano, 1997; Williams, 1989). Each receptor consists of an extracellular region harboring five immunoglobulin-like loops, a single transmembrane domain and an intracellular domain containing a split, catalytic tyrosine kinase (Williams, 1989). Ligand binding results in the dimerization of two PDGFRs to form PDGFRα homodimers, PDGFRα/β heterodimers or PDGFRβ homodimers (Fantauzzo and Soriano, 2016; Herren et al., 1993; Matsui et al., 1989; Seifert et al., 1989; Shim et al., 2010), followed by activation of the tyrosine kinase domains and trans-autophosphorylation of intracellular tyrosine residues (Herren et al., 1993; Kelly et al., 1991). Signaling molecules possessing Src homology 2 phosphotyrosine recognition motifs subsequently bind to phosphorylated residues in the intracellular domains of the receptors and initiate downstream signaling cascades (Heldin and Westermark, 1999; Williams, 1989). When expressed in the same cell type, signaling through the two receptors can result in different cell activities. For example, in the mouse cranial neural crest lineage, PDGFRα plays a predominant role in cranial neural crest cell migration, while PDGFRβ primarily contributes to proliferation of the cranial neural crest-derived facial mesenchyme (Mo et al., 2020). Given the structural similarities of PDGFRs and the fact that they interact with similar subsets of signaling molecules (Heldin and Westermark, 1999), a critical question is how this biological specificity is introduced to generate unique responses downstream of receptor engagement.

PDGFR internalization into the cell following ligand binding and dimerization also contributes to the regulation of PDGFR signaling (Bonifacino and Traub, 2003). Once internalized, PDGFRs can continue to bind adaptor proteins and/or signaling molecules within endosomes to activate downstream signaling pathways (Jastrzebski et al., 2017; Teis et al., 2002; Wang et al., 2004). Endosomal trafficking of the receptors commonly results in receptor degradation (Miyake et al., 1998; Miyake et al., 1999; Mori et al., 1995). However, two studies have demonstrated that PDGFRβ homodimers and PDGFRα/β heterodimers can also be recycled to the cell membrane (Hellberg et al., 2009; Karlsson et al., 2006), indicating potential dimer-specific differences in PDGFR trafficking following activation. Despite these findings, the dimer-specific dynamics of PDGFR activation, trafficking and signal attenuation, as well as the roles of these processes in mediating signal transduction and cellular activity, have not been studied in detail.

Here, we implemented bimolecular fluorescence complementation (BiFC) (Hu and Kerppola, 2003; Magliery et al., 2005) to probe for PDGFR dimer-specific dynamics. The BiFC technique adapted for this study employs a split Venus fluorescent protein (Croucher et al., 2016) fused to the C-terminus of individual PDGFRs to investigate receptor dimerization. This method overcomes limitations with prior approaches to examine receptor expression and/or dimerization using antibody-based methods that cannot distinguish between PDGFRs present as monomers or engaged in homodimers versus heterodimers. Here, we generated two stable cell lines – one for each PDGFR homodimer pair – expressing BiFC-tagged PDGFRs. The formation of a functional Venus fluorescent protein upon PDGFR dimerization allows for the visualization and purification of individual PDGFR dimers. Utilizing this technique, we demonstrated significant differences in the timing and extent of PDGFRα versus PDGFRβ homodimer dimerization, activation and trafficking, which lead to changes in downstream signaling and cellular activity. Taken together, these data shed considerable light on the mechanisms by which biological specificity is introduced downstream of PDGFR activation.

Results

Generation and validation of PDGFR-BiFC stable cell lines

To investigate PDGFR dimer-specific dynamics, we generated stable cell lines expressing BiFC-tagged PDGFRs. We cloned plasmids expressing C-terminal protein fusions of each PDGFR with BiFC fragments corresponding to the N-terminal (V1) or C-terminal (V2)

regions of the Venus fluorescent protein (Fig. S1A). Using lentiviral transduction of HCC15 cells (Fig. S1B-C'), we stably integrated PDGFR-BiFC sequences (PDGFRα-V1/PDGFRα-V2 and PDGFRβ-V1/PDGFRβ-V2) to generate two cell lines: a PDGFRα homodimer cell line and a PDGFRβ homodimer cell line, respectively. HCC15 cells were selected based on the lack of *PDGFR* expression, as the presence of endogenous PDGFRs would confound the interpretation of BiFC events. Further, these cells have little to no PDGF ligand expression, such that the BiFC-tagged PDGFRs would only be activated upon exogenous ligand stimulation. Finally, HCC15 cells express all the relevant adaptor proteins and signaling molecules known to function downstream of PDGFR activation (Barretina et al., 2012; Cancer Cell Line Encyclopedia and Genomics of Drug Sensitivity in Cancer, 2015; Heldin and Westermark, 1999). We confirmed that the relevant sequences were inserted into the genome via PCR amplification and Sanger sequencing. Next, we examined expression of transcripts encoding each receptor using quantitative real-time PCR (qRT-PCR), revealing similar expression of *PDGFRA* (6.49% ± 1.92% of *B2M* expression) and *PDGFRB* (14.8% ± 2.26% of *B2M* expression) in their respective cell lines (Fig. S1D). Interestingly, this ratio of *PDGFRA* to *PDGFRB* expression is comparable to the ratio of endogenous receptor expression previously reported in mouse embryonic fibroblasts, in which all three PDGFR dimers are active (Fantauzzo and Soriano, 2016). Finally, we established that the relevant PDGFR protein was expressed in each cell line and migrated at the expected height in SDS-PAGE (Fig. S1E,F). Within these cell lines, the individual N- and C-terminal fragments of the Venus fluorescent protein are expected to be non-fluorescent when bound to monomeric receptors. However, upon receptor dimerization, the N- and C-terminal fragments should co-localize, resulting in a functional Venus fluorescent protein. This BiFC event can be visualized through fluorescence microscopy or purified biochemically utilizing a GFP-Trap nanobody, which has an epitope that spans V1 and V2 (Croucher et al., 2016).

We initially starved the cells for 24 h in HITES medium, which lacks any growth factors, followed by fluorescence microscopy to determine baseline expression of Venus. For the PDGFRα homodimer cell line, the majority of Venus expression localized just outside of the nucleus (54%) (Fig. S1G,G'), with additional expression detected in the cytoplasm (21%), cell membrane (17%) and nucleus (8%). For the PDGFRβ homodimer cell line, Venus expression equally localized just outside of the nucleus (33%) (Fig. S1H,H') and within the nucleus (33%) (Fig. S1I,I'), with additional expression in the cell membrane (19%) and cytoplasm (14%). To

confirm the BiFC event and assess Venus expression upon exogenous ligand treatment, we starved the cells as above, photobleached the coverslips to ensure that all subsequent imaging captured newly-formed BiFC events and stimulated with PDGF ligand for 5 min. We stimulated PDGFRα homodimer cells with PDGF-AA ligand and PDGFRβ homodimer cells with PDGF-BB ligand, as previous data indicated that PDGFRα homodimers are primarily responsive to activation by PDGF-AA, while PDGFRβ homodimers are primarily activated by PDGF-BB (Bostrom et al., 1996; Ding et al., 2004; Fantauzzo and Soriano, 2016; Leveen et al., 1994; Soriano, 1994; Soriano, 1997). An important caveat to keep in mind, however, is that it is unclear if the ligands used in this study have the same affinities for their respective BiFC-tagged receptors. Amongst images with an average number of 15.4 cells for the PDGFRα homodimer cell line and 19.5 cells for the PDGFRβ homodimer cell line, we detected 1.45 (9.40%) and 1.53 (7.83%) Venus-positive cells, respectively. At this timepoint, Venus expression in the PDGFRα homodimer cell line was typically observed as small, internalized puncta, whereas in the PDGFRβ homodimer cell line, Venus expression was at both the cell membrane and inside the cell (Fig. 1A-D'). Quantification of fluorescence intensity revealed a significant increase in Venus intensity upon 5 min of ligand treatment for the two cell lines (PDGFRαV1/V2: $p = 0.0232$; PDGFRβV1/V2: $p = 0.0123$; Fig. 1E,F), with comparable fluorescence intensity between the two cell lines (PDGFRαV1/V2: 21.3 ± 2.79 arbitrary units (A.U.); PDGFRβV1/V2: 18.2 ± 1.12 A.U.; Fig. 1E,F).

Next, we investigated co-localization of the Venus signal with signal from anti-PDGFR antibodies. These data revealed that Venus signal co-localized with a subset of PDGFR expression at 5 min of ligand stimulation (Fig. 1G-J"). Pearson's correlation coefficient (PCC) for the Venus signal and PDGFR expression was similar between the PDGFRα homodimer (0.324 ± 0.0547 PCC) and the PDGFRβ homodimer cell lines (0.358 ± 0.0793 PCC; Fig. 1G,H). The regions of receptor expression that were not Venus-positive likely represent monomeric receptors and/or potential V1/V1 or V2/V2 dimers, which would not be expected to fluoresce (Fig. 1I-J"). The fact that we observed less than complete positive co-localization (PCC values <1) indicated that the presence of the BiFC fragments alone did not drive dimerization.

PDGFRβ receptors homodimerize more quickly than PDGFRα receptors

We further confirmed the BiFC event upon ligand treatment for both cell lines biochemically. Cells for both PDGFR homodimers were stimulated with PDGF ligand for 2, 5 and 15 min. Subsequent immunoprecipitation with the GFP-Trap nanobody was followed by western blotting for each receptor, normalizing the immunoprecipitation signal to the whole cell lysate signal. This revealed an increase in dimerized receptors following ligand treatment of both cell lines, with peak dimerization occurring at 5 min for both PDGFRα homodimers (1.25 ± 0.0361 relative induction (R.I.)) and PDGFRβ homodimers (1.49 ± 0.361 R.I.; Fig. 2A-C). Furthermore, PDGFRβ homodimers appeared to dimerize more quickly than PDGFRα homodimers, reaching near peak dimerization at 2 min of ligand treatment (1.47 ± 0.268 R.I.; Fig. 2C).

Next, we investigated the activation of both PDGFR homodimers by assessing receptor autophosphorylation. Each cell line was stimulated with PDGF ligand from 2 min to 4 h. Western blotting of whole cell lysates using an anti-phospho-PDGFR antibody revealed that both PDGFR homodimers were significantly and robustly autophosphorylated upon ligand treatment. Peak activation occurred at 5 min of ligand stimulation for PDGFRα homodimers (11.2 ± 2.44 R.I.) and at 15 min for PDGFRβ homodimers (28.2 ± 3.89 R.I.; Fig. 2D,E). Critically, there was very little to no activation of the PDGFRs in the absence of ligand (Fig. 2D), consistent with previous findings that both ligand binding and dimerization are required for receptor activation (Kelly et al., 1991; Yang et al., 2010). Furthermore, PDGFRβ homodimers exhibited more robust autophosphorylation than PDGFRα homodimers from 5 min to 4 h of PDGF ligand stimulation with significantly greater area under the curve ($p = 0.0003$; Fig. 2D,E). Together, these results suggested that PDGFRβ receptors homodimerize more quickly and have increased levels of autophosphorylation than PDGFRα homodimers.

Interestingly, each of the blots for total PDGFR protein levels revealed a doublet with a lower band at 170 kD (PDGFRα) or 180 kD (PDGFRβ) and an upper band at 190 kD (Fig. S1E,F; Fig. 2A,B,D). To determine whether the bands correspond to V1 and/or V2-tagged PDGFRs, we transiently transfected HEK 293T/17 cells with PDGFR-BiFC expression constructs. Each western blot lane had two bands (Fig. S2), likely representing the non-glycosylated and glycosylated versions of the PDGFRs (Shim et al., 2010). These bands ran slightly higher in the individual V1 lanes than the same bands in the individual V2 lanes (Fig. S2), which would be expected given the sizes of V1 (156 amino acids) and V2 (78 amino

acids). However, the anti-phospho-PDGFR blots revealed a single, upper band of 190 kD for both cell lines (Fig. 2D), indicating that only the glycosylated BiFC-tagged PDGFRs are phosphorylated upon PDGF ligand stimulation.

PDGFRα homodimers are trafficked more quickly and degraded faster, while PDGFRβ homodimers are more likely to be recycled

It is well-established that PDGFRs dimerize at the cell membrane upon ligand binding (Herren et al., 1993; Shim et al., 2010) and become internalized and trafficked in the cell following activation (De Donatis et al., 2008; Disanza et al., 2009; Miaczynska, 2013; Pahara et al., 2010; Rogers and Fantauzzo, 2020). To further investigate the different subcellular localization of Venus in the two cell lines following PDGF ligand treatment, we evaluated membrane localization of the PDGFR dimers at early timepoints of PDGF ligand treatment by measuring co-localization of the Venus signal with signal from an antibody recognizing the membrane marker Na^+/K^+-ATPase (Skou, 1989). We observed relatively similar levels of co-localization for PDGFRα homodimers and PDGFRβ homodimers at 1 and 2 min following PDGF ligand stimulation (Fig. 3A). At 5 min of ligand treatment, however, PDGFRα homodimer co-localization with Na^+/K^+-ATPase had decreased from a peak at 1 min, while PDGFRβ homodimers reached peak co-localization with the membrane marker (Fig. 3A-C"). To assess whether PDGFR dimer internalization could account for this comparative decrease in membrane localization for PDGFRα homodimers, we next measured the co-localization of the Venus signal with signal from an antibody recognizing the early endosome marker Rab5 (Zerial and McBride, 2001). These analyses revealed that PDGFRα homodimers co-localized significantly more with Rab5 at 2 min (0.250 ± 0.0316 PCC) and 5 min (0.215 ± 0.0310 PCC) of PDGF ligand treatment than PDGFRβ homodimers (0.123 ± 0.0192 PCC; $p = 0.0359$; 0.100 ± 0.0198 PCC; $p = 0.0440$, respectively), indicating a greater likelihood for PDGFRα homodimers to be trafficked at these timepoints (Fig. 3D-F"). Collectively, these data suggested that PDGFRα homodimers are trafficked more quickly, while PDGFRβ homodimers dwell at the membrane longer.

We next assessed trafficking of the PDGFR homodimers through late endosomes, which precedes trafficking to the lysosome for degradation (Mellman, 1996), by examining co-localization of the Venus signal with signal from an antibody recognizing the late endosome marker Rab7 (Zerial and McBride, 2001). These data revealed that PDGFRα homodimers co-

localized significantly more with Rab7 (0.280 ± 0.0111 PCC) than PDGFRβ homodimers (0.237 ± 0.00404 PCC; $p = 0.0474$) at 1 h of ligand treatment (Fig. 4A-C"). This finding suggested that PDGFRα homodimers may be degraded by lysosomes more quickly and/or to a greater extent than PDGFRβ homodimers. To investigate this further, we biochemically evaluated receptor degradation following PDGF ligand stimulation. We performed a 30 min pretreatment with cycloheximide to inhibit translation and then stimulated the cells with PDGF ligand from 2 min to 4 h. We collected cell lysates and performed western blotting for PDGFR levels in each condition. Following 4 h of ligand treatment, we observed 80% and 78% decreases from initial receptor levels for PDGFRα homodimers ($p = 0.0316$) and PDGFRβ homodimers, respectively, indicating a similar extent of degradation by the end of the timecourse (Fig. 4D,E). Importantly, we observed that PDGFRα homodimers were degraded at a quicker rate, particularly between 1 and 2 h (Fig. 4E), consistent with the Rab7 co-localization findings (Fig. 4A-C"). Taken together, these data suggested that PDGFRα homodimers are degraded more quickly than PDGFRβ homodimers.

To test whether the above receptor degradation is due to trafficking to the lysosome, we performed a 1 h pretreatment with the lysosome inhibitor chloroquine (Wiesmann et al., 1975) followed by a 30 min pretreatment with cycloheximide. Cells were stimulated with PDGF ligand and receptor levels were assessed via western blotting as described above. While the PDGFRα homodimer cell line showed no significant difference in receptor levels in the absence versus presence of chloroquine, there was a trend of increased receptor levels upon lysosome inhibition at 1, 2 and 4 h. In particular, the 1 h timepoint revealed a 19% increase in PDGFRα receptor levels in the presence of chloroquine (Fig. 4F,G). The PDGFRβ homodimer cell line exhibited a noticeable (42%) increase in PDGFRβ receptor levels at 1 h in the presence of chloroquine, as well as a significant difference in receptor levels in the absence (0.224 ± 0.0812 relative receptor levels (R.R.L.)) versus presence of chloroquine (0.534 ± 0.0734 R.R.L.; $p = 0.0479$) at 4 h (Fig. 4F,G). Collectively, these data suggested that trafficking to the lysosome contributes to PDGFR degradation following approximately 1 h of ligand treatment. Furthermore, while PDGFRα is degraded to a similar extent in the absence versus presence of chloroquine, indicating that it may primarily undergo proteasomal degradation in response to sustained ligand treatment, the second wave of PDGFRβ degradation appears to be almost exclusively lysosomal.

In contrast to being degraded, PDGFRs can alternatively be recycled to the membrane for continued signaling. To examine receptor recycling, we first quantified the co-localization of the Venus signal with signal from an antibody recognizing the rapid recycling endosome marker Rab4 (Zerial and McBride, 2001). Quantification indicated that PDGFRβ homodimers co-localized significantly more with Rab4 (0.224 ± 0.0131 PCC) than PDGFRα homodimers (0.167 ± 0.00765 PCC; $p = 0.0286$) at 15 min of ligand treatment (Fig. 5A-C"). Next, we examined co-localization of the Venus signal with signal from an antibody recognizing the slow recycling endosome marker Rab11 (Zerial and McBride, 2001). This analysis revealed that PDGFRβ homodimers co-localized significantly more with Rab11 (0.203 ± 0.0122 PCC) than PDGFRα homodimers (0.124 ± 0.0116 PCC; $p = 0.0094$) at 90 min of PDGF ligand treatment (Fig. 5D-F"). Consistently, at 90 min of PDGF ligand stimulation, PDGFRβ homodimers co-localized significantly more with the membrane marker Na^+/K^+-ATPase (0.150 ± 0.00680 PCC) than PDGFRα homodimers (0.101 ± 0.00722 PCC; $p = 0.0077$; Fig. S3A-C"). Taken together, these data demonstrated that PDGFRβ homodimers are more likely to be recycled back to the cell membrane through these rapid and slow recycling routes than PDGFRα homodimers.

PDGFRβ homodimer activation induces a greater amplitude of downstream signaling

We postulated that the differences in dimerization, activation and trafficking between PDGFR homodimers may affect downstream cell signaling. We performed a timecourse of ligand stimulation for each PDGFR homodimer cell line from 2 min to 4 h followed by western blotting for two well-studied effector molecules downstream of PDGFR activation: ERK1/2 and AKT (Fantauzzo and Soriano, 2016; Lemmon and Schlessinger, 2010; Vasudevan et al., 2015). Phosphorylation of ERK1/2 in response to PDGFRα homodimer signaling peaked at 15 min following PDGF ligand stimulation (1.50 ± 0.236 R.I.) and remained relatively stable throughout the timecourse (1.33 ± 0.0693 R.I. at 4 h; Fig. 6A,B). Phosphorylation of ERK1/2 in response to PDGFRβ homodimer signaling displayed a similar curve to that of PDGFRα homodimers but initially peaked later, at 30 min of PDGF stimulation (2.32 ± 0.581 R.I.), with a higher amplitude than the PDGFRα homodimers (Fig. 6A,B). Phosphorylation of AKT in response to PDGFRα homodimer activation initially peaked at 15 min of ligand treatment (2.04 ± 0.284 R.I.; $p = 0.0382$) and, comparable to the phosphorylation dynamics of ERK1/2, remained relatively stable (2.30 ± 0.556 R.I. at 4 h; Fig. 6C,D). Phosphorylation of AKT in response to PDGFRβ homodimer activation also peaked at 15 min of ligand stimulation (5.85 ±

1.25 R.I.; p = 0.0165) but had a greater amplitude than PDGFRα homodimers and appeared more dynamic, sharply declining after the peak at 15 min (Fig. 6C,D). These signaling data suggested that PDGFR homodimers differ in downstream signaling dynamics and that PDGFRβ homodimers generate a greater signaling response to PDGF ligand stimulation than PDGFRα homodimers.

An important question is whether these differences in signaling downstream of the PDGFR homodimers were due to innate differences in the clones that we chose for each of these cell lines, rather than differences in signaling activity downstream of PDGFRα versus PDGFRβ homodimers. We tested this question through activation of an alternate RTK, EGFR. We stimulated each cell line with EGF for 10 min and performed western blotting for the phosphorylation of the same effector molecules, revealing no difference in phosphorylation of ERK1/2 and AKT between the PDGFR homodimer cell lines (Fig. S4A-D). These results indicated that the differences that we observed upon PDGF ligand stimulation of our two PDGFR homodimer cell lines reflect true differences in signaling response downstream of these receptors.

Inhibition of clathrin-mediated endocytosis results in alterations in cellular trafficking and downstream signaling dynamics, especially for PDGFRα homodimers

To test the requirement for PDGFR endocytosis in downstream cell signaling, we performed a 1 h pretreatment with Dyngo-4a, which inhibits the large GTPase dynamin from pinching off clathrin-coated vesicles from the cell membrane (McCluskey et al., 2013; Sadowski et al., 2013). In this case, PDGFRα homodimer co-localization with Rab5 at 2 min of PDGF ligand treatment (0.121 ± 0.0175 PCC; Fig. 7A,B-B'') was significantly reduced from its previous value (p = 0.0350) to a level similar to that of PDGFRβ homodimers (0.137 ± 0.0135 PCC; Fig. 7A,C-C''). Furthermore, treatment with Dyngo-4a resulted in distinct changes in signaling downstream of each PDGFR homodimer. PDGFRα homodimers exhibited delayed phosphorylation of ERK1/2 in response to PDGF ligand following dynamin inhibition, with relative induction remaining below baseline levels until 1 h or more of ligand stimulation and peaking at 4 h (1.37 ± 0.518 R.I.; Fig. 7D,E). Alternatively, the early phosphorylation dynamics of ERK1/2 in response to PDGFRβ homodimer activation were not affected by dynamin inhibition, peaking at 30 min of ligand stimulation (2.47 ± 0.442 R.I.; Fig. 7D,E) as in non-Dyngo-4a experiments. Similar to the phosphorylation of ERK1/2, phosphorylation of AKT in

response to PDGFRα homodimer activation exhibited significantly reduced induction at 15 min (p = 0.0311) and 30 min (p = 0.0194) of PDGF ligand stimulation following dynamin inhibition compared to non-Dyngo-4a experiments, with relative induction remaining below baseline levels until 1 h or more of ligand stimulation and peaking at 4 h (1.60 ± 0.0529 R.I.; Fig. 7F,G). Comparably, phosphorylation of AKT in response to PDGFRβ homodimer activation also peaked at a later timepoint of 1 h of ligand stimulation (4.22 ± 1.10 R.I.). Taken together, these data demonstrated that inhibition of clathrin-mediated endocytosis results in alterations in cellular trafficking and downstream signaling dynamics for PDGFR homodimers, with a greater impact on PDGFRα than PDGFRβ.

PDGFRβ homodimer activation leads to greater cellular activity

As with many RTKs, signaling through the PDGFRs has been shown to direct a range of cellular processes (Fantauzzo and Soriano, 2015; Schlessinger, 2000). To determine how the above trafficking and signaling dynamics of the PDGFR homodimers affect cellular activity, we first measured proliferation via a soft agar anchorage-independent growth assay in growth medium with 10% fetal bovine serum. In the absence of ligand, the cells expressing PDGFRβ proliferated significantly more than those expressing PDGFRα, as measured by colony area ($7.80 \times 10^5 \pm 4.72 \times 10^4$ versus $3.32 \times 10^5 \pm 4.81 \times 10^4$ A.U.; p = 0.0027; Fig. 8A,B,D). Upon exogenous PDGF ligand stimulation, proliferation as measured by colony count increased for the PDGFRα homodimer cell line ($8.60 \times 10^3 \pm 8.77 \times 10^2$ versus $7.43 \times 10^3 \pm 8.59 \times 10^2$ colonies; p = 0.0074; Fig. 8A,A',C) and proliferation as measured by colony area increased for the PDGFRβ homodimer cell line ($8.92 \times 10^5 \pm 4.44 \times 10^4$ versus $7.80 \times 10^5 \pm 4.72 \times 10^4$ A.U.; p = 0.0325; Fig. 8B,B',D). Finally, the cells expressing PDGFRβ proliferated significantly more than those expressing PDGFRα upon exogenous ligand treatment, as measured by colony area ($8.92 \times 10^5 \pm 4.44 \times 10^4$ versus $3.81 \times 10^5 \pm 6.63 \times 10^4$ A.U.; p = 0.0048; Fig. 8A',B',D). These effects were confirmed via immunofluorescence analysis using the proliferation marker Ki67 (Gerdes et al., 1984) (Fig. S5A-B'). Here, both cell lines exhibited trends for increased proliferation upon exogenous PDGF ligand stimulation, with cells expressing PDGFRβ proliferating more than those expressing PDGFRα in the absence and presence of ligand (Fig. S5C). We next performed 24 h transwell migration assays in growth medium with 10% fetal bovine serum to assess cell migration for the two PDGFR homodimer cell lines. Only the PDGFRβ homodimer cell line exhibited increased migration towards growth medium containing

PDGF ligand ($3.14 \times 10^8 \pm 3.22 \times 10^7$ versus $1.24 \times 10^8 \pm 1.59 \times 10^7$ A.U.; $p = 0.0022$; Fig. 8F,F',G). Further, addition of exogenous ligand resulted in increased migration for cells expressing PDGFRβ over those expressing PDGFRα ($3.14 \times 10^8 \pm 3.22 \times 10^7$ versus $2.07 \times 10^8 \pm 2.14 \times 10^7$ A.U.; $p = 0.0218$; Fig. 8E',F',G).

To confirm these results in a physiologically-relevant setting in which both PDGFRα and PDGFRβ are endogenously expressed, we cultured primary mouse embryonic palatal mesenchyme (MEPM) cells derived from the palatal shelves of embryonic day 13.5 *Pdgfra*$^{fl/fl}$*;Wnt1-Cre*$^{+/Tg}$ or *Pdgfrb*$^{fl/fl}$*;Wnt1-Cre*$^{+/Tg}$ embryos (Fantauzzo and Soriano, 2016). We reasoned that PDGF-AA ligand treatment of *Pdgfrb*$^{fl/fl}$*;Wnt1-Cre*$^{+/Tg}$ cells could only activate PDGFRα homodimers, while PDGF-BB ligand treatment of *Pdgfra*$^{fl/fl}$*;Wnt1-Cre*$^{+/Tg}$ cells could only activate PDGFRβ homodimers. Confirming the results from the HCC15-based stable cell lines, upon exogenous PDGF ligand stimulation, the cells expressing PDGFRβ proliferated significantly more than those expressing PDGFRα in both starvation medium containing 0.1% FBS (0.200 ± 0.0148 versus 0.0778 ± 0.0115; $p = 0.0006$; Fig. S6A) and growth medium containing 10% FBS (0.317 ± 0.0318 versus 0.137 ± 0.0326; $p = 0.0056$; Fig. S6A). Similarly, the cells expressing PDGFRβ migrated significantly more than those expressing PDGFRα in the presence of exogenous PDGF ligand ($4.89 \times 10^4 \pm 1.59 \times 10^3$ versus $2.64 \times 10^4 \pm 4.02 \times 10^3$; $p = 0.0193$; Fig. S6B-D). Collectively, these cellular activity assays provided evidence that activated PDGFRβ homodimers generate stronger pro-proliferation and pro-migration signals than PDGFRα homodimers.

Discussion

It has previously been impossible to investigate PDGFR dimer-specific dynamics. Former studies utilized antibody- and ligand propensity-based approaches to study PDGFR expression and/or activity, yet both approaches have considerable caveats. Antibodies cannot distinguish whether a receptor is present as a monomer or engaged in a homodimeric or heterodimeric complex. Proximity ligation techniques are also insufficient, as they detect protein-protein interactions within a relatively large range of 40 nm (Bagchi et al., 2015), while dimerized PDGFRs may have considerably closer interactions (Chen et al., 2015). Moreover, evidence suggests that some PDGF ligands are promiscuous and can result in the formation of multiple PDGFR dimers (Fantauzzo and Soriano, 2016). Therefore, in studies where

conclusions were drawn about a particular PDGFR dimer based on ligand treatment alone, it is often unclear which dimer was assayed. Our aim was to implement an optimized method, BiFC, to both visualize and purify individual PDGFR dimers to more precisely investigate homodimer-specific subcellular distribution and signaling dynamics. We observed less than complete co-localization between Venus and PDGFR antibody expression, demonstrating that PDGFR expression is not predictive of receptor dimerization and activation, and further indicating that the presence of the BiFC fragments alone does not drive dimerization in our cell lines.

Interestingly, we took multiple approaches to generate a PDGFRαV1/βV2 stable cell line, with limited success. A single clone expressing both receptors was obtained among 188 clones screened. However, despite two rounds of subcloning, the frequency of BiFC events remained surprising low. Relatedly, qRT-PCR analyses revealed that expression of *PDGFRA* and *PDGFRB* was approximately 4-fold and 13-fold lower, respectively, in this clone compared to our PDGFRα and PDGFRβ homodimer cell lines. Moreover, the cells grew very slowly compared to parental HCC15 cells and both PDGFRα and PDGFRβ homodimer cell lines. Taken together, we have concluded that HCC15 cells do not tolerate combined expression of PDGFRα and PDGFRβ, and/or formation of PDGFRα/β heterodimers.

Our initial characterization of Venus expression in the absence of photobleaching and PDGF ligand treatment for the PDGFR homodimer cell lines indicated some baseline BiFC expression. This Venus expression is likely due to low levels of PDGF ligand expressed by HCC15 cells and/or PDGFR homodimer formation in the absence of ligand stimulation. Similarly, our GFP-Trap purification of the PDGFR homodimers revealed increased dimerization for both upon PDGF ligand stimulation, as well as, surprisingly, the presence of dimerized receptors in the absence of ligand stimulation. As recently discussed, an *in silico* study has implicated that there may be an inactive dimerization state for the PDGFRs (Polyansky et al., 2019; Rogers and Fantauzzo, 2020). Interestingly, other RTKs, most notably EGFR, have been shown to exist in an inactive dimerized state in the membrane prior to a ligand-induced conformational change (Bae and Schlessinger, 2010; Zhang et al., 2006). Importantly, even though we detected dimerized PDGFRs in the absence of ligand stimulation, we revealed that PDGFR homodimers were only activated upon exogenous ligand treatment.

In studying these receptor dimerization and activation dynamics, we observed that PDGFRβ receptors dimerized more quickly than PDGFRα receptors. On the other hand, PDGFRα homodimers reached their peak autophosphorylation faster than PDGFRβ

homodimers, though the PDGFRα peak was significantly lower than that for PDGFRβ. It is possible that these trends in dimerization and activation may be due to different conformations of the receptors prior to and during activation. There is precedent for this concept in the RTK field, as the extracellular regions of ErbB family members EGFR, ErbB3 and ErbB4 possess an intramolecular tether in the absence of ligand binding that buries the dimerization arm of the cysteine-rich 1 subdomain (Bouyain et al., 2005; Cho and Leahy, 2002; Ferguson et al., 2003), while ErbB2 exists in an extended conformation that exposes both cysteine-rich subdomains (Cho et al., 2003; Garrett et al., 2003). A similar explanation for the differences in autophosphorylation activity between the PDGFR homodimers may be the auto-inhibitory function of a glutamic acid/proline repeat motif in the C-terminal tail of PDGFRβ (Chiara et al., 2004), which is alleviated upon ligand-induced dimerization and conformational change of the receptor. As this motif has not been detected in PDGFRα, it could create a relative delay in activation for PDGFRβ compared to PDGFRα homodimers.

Our PDGFR homodimer dimerization and activation findings are noteworthy in the context of the Na^+/K^+-ATPase and Rab5 co-localization data, from which we determined that PDGFRα homodimers are trafficked from the cell membrane more quickly than PDGFRβ homodimers. Additionally, as discussed above, we demonstrated that PDGFRβ homodimers are activated to a greater extent than PDGFRα homodimers. It may be the case that the extended time at the cell membrane for the PDGFRβ homodimers allows for increased autophosphorylation. Conversely, earlier peak activation of the PDGFRα homodimers may result in faster recruitment of trafficking machinery and, thus, quicker intracellular trafficking. It is also possible that dimer conformation may play a role in these internalization and trafficking dynamics, though the complete conformations of the PDGFR homodimers remain unknown. Molecules that post-translationally modify both PDGFRα and PDGFRβ to recruit endosomal machinery, such as the RING-finger E3 ubiquitin ligase Cbl, likely fine-tune these dynamics (Reddi et al., 2007; Rorsman et al., 2016; Schmid et al., 2018). Furthermore, PDGFRβ has a known internalization motif located in the C-terminal domain of the receptor (Mori et al., 1991; Pahara et al., 2010), while such a motif has yet to be uncovered for PDGFRα, potentially imparting unique internalization and trafficking mechanisms for the various PDGFR dimers.

In addition to differences in the timing of initial PDGFR trafficking into early endosomes, our data also revealed varied degradation dynamics and recycling between the PDGFR dimers. We found that PDGFRα homodimers co-localized more with Rab7 following 1 h of

PDGF ligand stimulation and were degraded faster than PDGFRβ homodimers shortly afterwards. However, both PDGFR homodimers experienced similar levels of receptor degradation following 4 h of ligand treatment. We further demonstrated that lysosomal inhibition partially alleviated both PDGFRα and PDGFRβ degradation following 1 h of PDGF ligand treatment, indicating an early wave of lysosomal degradation for both homodimers. Notably, while lysosomal inhibition had little effect on PDGFRα levels after 4 h of ligand treatment, it significantly increased PDGFRβ levels, suggesting later waves of proteasomal and lysosomal degradation for PDGFRα and PDGFRβ, respectively. These findings align with prior results demonstrating the relevance of both degradation pathways for PDGFRs (Li et al., 2017; Mori et al., 1995; Reddi et al., 2007; Rorsman et al., 2016). We additionally found that PDGFRβ homodimers were more likely to be recycled than PDGFRα homodimers. However, the fact that only 20-22% of initial receptor levels for both cell lines were detected following 4 h of PDGF ligand treatment indicated that receptor degradation is the predominant result of intracellular trafficking, consistent with previous findings for PDGFRβ (Hellberg et al., 2009; Sadowski et al., 2013).

We next sought to determine how these dimerization and activation dynamics, together with PDGFR dimer-specific subcellular distribution, affected downstream signaling. We found that both PDGFR homodimers induced phospho-ERK1/2 peaks that remained relatively stable over time. PDGFRα homodimers drove an early peak of ERK1/2 phosphorylation, while the peak driven by PDGFRβ homodimer activation occurred slightly later and had a higher amplitude. Interestingly, it has previously been shown that various subcellular localizations of Erk1/2, or its upstream activator RAS, result in different timing of the Erk1/2 signaling response (Bruggemann et al., 2021; Herrero et al., 2016; Keyes et al., 2020). For example, following EGF ligand stimulation, the phosphorylation of Erk1/2 at the membrane results in sustained signaling, while its phosphorylation in the cytoplasm and nucleus results in transient signaling, ultimately leading to differences in cellular activity (Keyes et al., 2020). Given that PDGFRs have been shown to signal within various cellular compartments, including endosomes (Wang et al., 2004), engagement of signaling molecules at different subcellular locations may explain, at least in part, the observed differences in ERK1/2 signaling dynamics downstream of PDGFRα versus PDGFRβ homodimer activation. Correspondingly, the trends of AKT phosphorylation were also different between the two PDGFR homodimers. Though initial phospho-AKT peaks occurred at a similar timepoint for both PDGFR homodimers, the

PDGFRα homodimer-driven peak remained relatively stable, while PDGFRβ homodimer-stimulated phosphorylation of AKT was much more transient. In line with the phospho-ERK1/2 results, PDGFRβ homodimer activation induced a greater level of phospho-AKT than PDGFRα homodimers, suggesting that signaling through PDGFRβ homodimers results in greater activation of downstream signaling cascades.

Interestingly, two previous studies have suggested that activation of PDGFRα/β heterodimers leads to a greater MAPK downstream signaling response than that of either PDGFR homodimer. In the first, a porcine aortic endothelial cell line stably expressing exogenous PDGFRα and PDGFRβ was treated with PDGF-AB and PDGF-BB ligand. Stimulation with PDGF-AB ligand, which was proposed to generate PDGFRα/β heterodimers, led to reduced phosphorylation at Y771 in the cytoplasmic domain of PDGFRβ in comparison to PDGF-BB ligand treatment, which was proposed to more efficiently activate PDGFRβ homodimers. This reduced phosphorylation led to decreased association of PDGFRβ with a negative MAPK regulator, RasGAP, and increased downstream Ras and ERK2 activation (Ekman et al., 1999). In a second study comparing PDGF-AA, PDGF-BB and PDGF-DD ligand treatment of mouse embryonic fibroblasts, PDGF-BB ligand led to the greatest physical association of PDGFRα and PDGFRβ receptors and induced the highest peak of phospho-Erk1/2 signal (Fantauzzo and Soriano, 2016). However, in each case, it cannot be ruled out that multiple PDGFR dimers formed in response to ligand treatment and contributed to the downstream signaling response. Thus, the signaling dynamics downstream of PDGFRα/β heterodimer activation, and how these dynamics compare to those detected upon PDGFR homodimer activation, remain to be determined.

Importantly, inhibition of clathrin-mediated endocytosis indicated a particular requirement for rapid internalization and trafficking of PDGFRα homodimers in the propagation of downstream signaling. The observed difference in AKT phosphorylation following PDGFRα homodimer activation between untreated versus Dyngo-4a-treated conditions is particularly noteworthy, as PDGFRα homodimers have been shown to predominantly signal through the PI3K/Akt pathway during development (Klinghoffer et al., 2002). These findings support a model in which differences in the timing and extent of PDGFR homodimer internalization and trafficking fine tune downstream signaling responses. An important consideration, however, is that we evaluated whole cell lysates reflecting population-level dynamics, and it is likely that these dynamics differ between individual cells (Sparta et al., 2015).

Finally, cell activity assays revealed that PDGF ligand stimulation of PDGFRβ homodimers resulted in increased levels of both proliferation and migration from what was observed upon PDGFRα homodimer activation. The duration of Erk1/2 signaling downstream of RTK activation has been shown to determine cellular responses in various settings, with transient signaling resulting in proliferation and sustained signaling leading to differentiation or migration (Bruggemann et al., 2021; Freed et al., 2017; Marshall, 1995). Given the relatively sustained ERK1/2 signaling downstream of PDGFRβ homodimer activation, it is interesting that both proliferation and migration were stimulated. Whether the differences in cellular responses that we observed downstream of PDGFRα versus PDGFRβ homodimers stem from varying responses to a relatively low PDGF ligand concentration and/or inherent differences in the enzymatic activity of the homodimers remain to be determined. In support of the former hypothesis, varying concentrations of PDGF ligand have been shown to result in differences in both PDGFR trafficking and downstream proliferation and migration (De Donatis et al., 2008). Future signaling and cell activity studies will incorporate a range of PDGF ligand concentrations. Alternatively, activation of PDGFRβ homodimers may generate stronger kinase activity than that of PDGFRα homodimers. In fact, analysis of chimeric PDGFRs *in vivo* revealed that the intracellular domain of PDGFRβ can compensate for the loss of PDGFRα signaling, while the inverse is not true (Klinghoffer et al., 2001). Both hypotheses considered, it remains that PDGFRβ homodimers stimulated increased cell activity upon exogenous PDGF ligand stimulation in the context of both HCC15 cells and primary MEPM cells. However, we cannot rule out that the higher expression of *PDGFRB* than that of *PDGFRA* in the PDGFR-BiFC-HCC15 cell lines contributed, at least in part, to the differences in signaling and cell activity dynamics that we observed between the two homodimer cell lines.

Overall, we have identified PDGFR homodimer-specific differences in dimerization, activation, trafficking, downstream signaling and cellular activity utilizing a novel BiFC system. Our findings thus provide significant insight into how similar receptors within an RTK family utilize a combination of mechanisms to differentially propagate downstream signaling. This approach will be invaluable in future studies characterizing PDGFR dimer-specific interactomes to further delineate the means by which these receptors generate distinct cellular outputs.

Materials and methods

Generation of PDGFR-BiFC-HCC15 cell lines

Using Gateway cloning, we cloned pDONOR223-PDGFRA (23892; Addgene, Watertown, MA, USA) and pDONOR223-PDGFRB (23893; Addgene) each into pDEST-ORF-V1 (73637; Addgene) and, separately, into pDEST-ORF-V2 (73638; Addgene). PDGFRα-V1, PDGFRα-V2, PDGFRβ-V1 and PDGFRβ-V2 sequences were amplified by PCR using the following primers (Integrated DNA Technologies, Inc., Coralville, IA, USA): 5'-TTACTCGAGATGGGGACTTCCCATCCGGC-3' and 5'-TTACCCGGGTTACTGCTTGTCGGCGGTGA-3', 5'-TTACTCGAGATGGGGACTTCCCATCCGGC-3' and 5'-TTACCCGGGTTACTTGTACAGCTCGTCCA-3', 5'-TTAGAATTCATGCGGCTTCCGGGTGCGAT-3' and 5'-CTGTCTAGATTACTGCTTGTCGGCGGTGA-3', 5'-TTAGAATTCATGCGGCTTCCGGGTGCGAT-3' and 5'-CGGTCTAGATTACTTGTACAGCTCGTCCA-3', respectively. The sequences were cloned into the pLVX-Puro vector using XhoI and XmaI sites for PDGFRα-V1 and PDGFRα-V2 and EcoRI and XbaI sites for PDGFRβ-V1 and PDGFRβ-V2. The above lentiviral constructs (10 mg) and packaging vectors pCMV-VSV-G (Stewart et al., 2003) and pCMV-dR8.91 (Zufferey et al., 1997) (5 mg each) were transfected into HEK 293T/17 cells using Lipofectamine LTX (Thermo Fisher Scientific, Waltham, MA, USA). Medium containing lentivirus was collected 48 h and 72 h following transfection and filtered using a 13 mm syringe filter with a 0.45 μm PVDF membrane (Thermo Fisher Scientific) following addition of 4 mg/mL polybrene (Sigma-Aldrich, St. Louis, MO, USA). Lentiviral-containing medium was added to HCC15 lung cancer cells every 24 h for two days, and cells were subsequently grown in the presence of 2 μg/mL puromycin for 10 days. Individual Venus-positive cells were isolated on a Moflo XDP 100 cell sorter (Beckman Coulter Inc., Brea, CA, USA) following 5 min of stimulation with 10 ng/mL PDGF-AA or PDGF-BB (R&D Systems, Minneapolis, MN, USA) for the PDGFRα homodimer and PDGFRβ homodimer cell lines, respectively, and expanded to generate clonal cell lines. Final clones chosen for PDGFRα and PDGFRβ homodimer cell lines were confirmed by PCR amplification of the inserted sequences from genomic DNA using primers found in Table S1. These PCR products were subcloned into the Zero Blunt TOPO vector (Thermo Fisher Scientific) and Sanger sequenced.

PDGFR-BiFC-HCC15 cell culture

The HCC15 lung cancer cell line was obtained from the laboratory of Dr. Lynn Heasley. The cell line was authenticated through short tandem repeat analysis and tested for mycoplasma contamination every 10 passages using the MycoAlert Mycoplasma Detection Kit (Lonza Group Ltd, Basel, Switzerland). PDGFR-BiFC stable cells were cultured in RPMI growth medium [RPMI (Gibco, Thermo Fisher Scientific) supplemented with 100 U/mL penicillin (Gibco), 100 μg/mL streptomycin (Gibco) containing 10% FBS (Hyclone Laboratories Inc., Logan, UT, USA)] at 37ºC in 5% carbon dioxide. Once the stable cell lines were established, they were split at a ratio of 1:5 for maintenance. PDGFRα homodimer cells were used for experiments at passages 6-19, and PDGFRβ homodimer cells were used for experiments at passages 10-23. When serum starved, cells were grown in HITES medium [DMEM/F12 (Corning, Corning, NY, USA) supplemented with 0.1% bovine serum albumin (Fisher Scientific, Thermo Fisher Scientific), 10 mM beta-estradiol (Sigma-Aldrich), 10 mM hydrocortisone (Sigma-Aldrich), 5 μg/mL insulin (Sigma-Aldrich), 100 U/mL penicillin (Gibco), 100 μg/mL streptomycin (Gibco), 1.2 mg/mL $NaHCO_3$ (Santa Cruz Biotechnology, Inc., Dallas, TX, USA), 30 nM Na_3SeO_3 (Sigma-Aldrich) and 10 μg/mL apo-transferrin (Sigma-Aldrich)].

qRT-PCR

Total RNA was isolated using the RNeasy Mini Kit (Qiagen, Germantown, MD, USA) according to the manufacturer's instructions. First-strand cDNA was synthesized using a ratio of 2:1 random primers:oligo (dT) primer and SuperScript II RT (Invitrogen, Thermo Fisher Scientific) according to the manufacturer's instructions. qRT-PCR was performed on a CFX Connect Real-Time PCR Detection System and analyzed with CFX Manager software (version 3.1; Bio-Rad Laboratories, Inc., Hercules, CA, USA). All reactions were performed with SYBR Select Master Mix (Applied Biosystems, Thermo Fisher Scientific), 300 nM primers (Integrated DNA Technologies, Inc.) and cDNA in a 20 μL reaction volume. PCR primers for qRT-PCR analyses can be found in Table S2. The following PCR protocol was used: step 1, 2 min at 50ºC; step 2, 2 min at 95ºC; step 3, 15 sec at 95ºC; step 4, 1 min at 60ºC; repeat steps 3 and 4 for 39 cycles; step 5 (melting curve), 5 sec per 0.5ºC increment from 65ºC to 95ºC. All samples were run in triplicate and normalized against an endogenous internal control, *B2M*. qRT-PCR experiments were performed across three independent experiments, each using a separate passage of cells.

Immunoprecipitations and western blotting

PDGFR-BiFC-HCC15 cells were cultured as described above. To induce PDGFRα homodimer or PDGFRβ homodimer signaling, PDGFRα homodimer cells and PDGFRβ homodimer cells at ~60-70% confluence were serum starved for 24 h in HITES medium and stimulated with 10 ng/mL PDGF-AA or PDGF-BB ligand (R&D Systems), respectively, for the indicated length of time. To induce epidermal growth factor receptor (EGFR) signaling, cells were similarly stimulated with 10 ng/mL EGF (PeproTech, Thermo Fisher Scientific). When applicable, cells were pretreated with 10 μg/mL cycloheximide (Sigma-Aldrich) in DMSO (or an equivalent volume of DMSO) for 30 min before PDGF ligand stimulation and/or chloroquine (Sigma-Aldrich) in water (or an equivalent volume of water) for 1 h before PDGF ligand stimulation; or 30 μM Dyngo-4a (Abcam, Waltham, MA, USA) in DMSO (or an equivalent volume of DMSO) for 1 h before PDGF ligand stimulation. Protein lysates for immunoprecipitation were generated by resuspending cells in ice-cold GFP-Trap lysis buffer [20 mM Tris-HCl (pH 7.5), 150 mM NaCl, 0.5% Nonidet P-40, 1 mM EDTA, 1× complete Mini protease inhibitor cocktail (Roche, MilliporeSigma, Burlington, MA, USA), 1 mM PMSF] and collecting cleared lysates by centrifugation at 13,400 g at 4ºC for 20 min. For immunoprecipitations, cell lysates (500 μg) were incubated with GFP-Trap agarose beads (Bulldog Bio, Inc., Portsmouth, NH, USA) for 1 h at 4ºC. Beads were washed three times with ice-cold GFP-Trap wash/dilution buffer [10 mM Tris HCl (pH 7.5), 150 mM NaCl, 0.5 M EDTA] and the precipitated proteins were eluted with Laemmli buffer containing 10% β-mercaptoethanol, heated for 10 min at 100ºC and separated by SDS-PAGE. For western blotting analysis of whole cell lysates, protein lysates were generated by resuspending cells in ice-cold NP-40 lysis buffer [20 mM Tris-HCl (pH 8), 150 mM NaCl, 10% glycerol, 1% Nonidet P-40, 2 mM EDTA, 1× complete Mini protease inhibitor cocktail (Roche), 1 mM PMSF, 10 mM NaF, 1 mM Na_3VO_4, 25 mM β-glycerophosphate] and collecting cleared lysates by centrifugation at 13,400 g at 4ºC for 20 min. Laemmli buffer containing 10% β-mercaptoethanol was added to the lysates, which were heated for 5 min at 100ºC. Proteins were subsequently separated by SDS-PAGE. Western blot analysis was performed according to standard protocols using horseradish peroxidase-conjugated secondary antibodies. Full, uncropped western blots are provided in Fig. S7. The following antibodies were used for western blotting: PDGFRα (1:200; C-20; sc338; Santa Cruz Biotechnology, Inc.) (validation, dimerization and receptor degradation experiments); PDGFRβ (1:200; 958; sc432; Santa Cruz Biotechnology,

Inc.) (validation, dimerization and receptor degradation experiments); β-tubulin (1:1000; E7; E7; Developmental Studies Hybridoma Bank, Iowa City, IA, USA); phospho-PDGFRα (Tyr 849)/PDGFRβ (Tyr857) (1:1000; C43E9; 3170; Cell Signaling Technology, Inc., Danvers, MA, USA); PDGFRα (1:1000; D13C6; 5241; Cell Signaling Technology, Inc.) (autophosphorylation and chloroquine experiments); PDGFRβ (1:1000; 28E1; 3169; Cell Signaling Technology, Inc.) (autophosphorylation and chloroquine experiments); phospho-Erk1/2 (1:1000; Thr202/Thr204; 9101; Cell Signaling Technology, Inc.); Erk1/2 (1:1000; 9102; Cell Signaling Technology, Inc.); phospho-Akt (1:1000; Ser473; 9271; Cell Signaling Technology Inc.); Akt (1:1000; 9272; Cell Signaling Technology Inc.); horseradish peroxidase-conjugated goat anti-rabbit IgG (1:20,000; 111035003; Jackson ImmunoResearch Inc., West Grove, PA, USA); horseradish peroxidase-conjugated goat anti-mouse IgG (1:20,000; 115035003; Jackson ImmunoResearch Inc.). Quantifications of signal intensity were performed with ImageJ software (version 1.52a, National Institutes of Health, Bethesda, MD, USA). Relative dimerized PDGFR levels were determined by normalizing GFP-Trap immunoprecipitated PDGFR levels to total PDGFR levels. Relative phospho-PDGFR levels were determined by normalizing to total PDGFR levels. Relative degraded PDGFR levels were determined by normalizing cycloheximide-treated or chloroquine and cycloheximide-treated PDGFR levels to DMSO-treated or water and DMSO-treated PDGFR levels. Relative phospho-ERK1/2 levels were determined by normalizing to total ERK1/2 levels. Relative phospho-AKT levels were determined by normalizing to total AKT levels. When applicable, statistical analyses were performed with Prism 9 (GraphPad Software Inc., San Diego, CA, USA) using a two-tailed, ratio paired *t*-test within each cell line (comparing individual ligand treatment timepoint values to the no ligand 0 min timepoint value) and a two-tailed, unpaired *t*-test with Welch's correction between each cell line or within each cell line comparing treatments. Immunoprecipitation and western blotting experiments were performed across at least three independent experiments.

Fluorescence analysis

For fluorescence intensity and marker co-localization experiments, cells were seeded onto glass coverslips coated with 5 μg/mL human plasma fibronectin purified protein (MilliporeSigma) at a density of 80,000 cells and 40,000 cells for the PDGFRα homodimer cell line and PDGFRβ homodimer cell line, respectively, in RPMI growth medium. 24 h later, cells were washed with 1x phosphate buffered saline (PBS) and serum starved in HITES medium.

HITES medium was replaced 23 h later. After 54 min, coverslips were photobleached for 1 min with an Axio Observer 7 fluorescence microscope (Carl Zeiss Microscopy LLC, White Plains, NY, USA) using the 2.5x objective and 488 nm laser. Cells were allowed to recover for 5 min and were treated with 10 ng/mL PDGF-AA or PDGF-BB ligand (R&D Systems) for the indicated amount of time. When applicable, cells were pretreated with 30 μM Dyngo-4a (Abcam) in DMSO (or an equivalent volume of DMSO) for 1 h before PDGF ligand stimulation. Cells were fixed in 4% paraformaldehyde (PFA) in PBS with 0.1% Triton X-100 for 10 min and washed in PBS. Cells were blocked for 1 h in 5% normal donkey serum (Jackson ImmunoResearch Inc.) in PBS and incubated overnight at 4ºC in primary antibody diluted in 1% normal donkey serum in PBS. After washing in PBS, cells were incubated in Alexa Fluor 546-conjugated donkey anti-rabbit secondary antibody (1:1,000; A21206; Invitrogen) or Alexa Fluor 546-conjugated donkey anti-mouse secondary antibody (1:1,000; A10036; Invitrogen) diluted in 1% normal donkey serum in PBS with 2 μg/mL 4',6-diamidino-2-phenylindole (DAPI; Sigma-Aldrich) for 1 h. Cells were mounted in either VECTASHIELD HardSet Antifade Mounting Medium or VECTASHIELD Vibrance Antifade Mounting Medium (Vector Laboratories, Inc., Burlingame, CA, USA) and photographed using an Axiocam 506 mono digital camera (Carl Zeiss Microscopy LLC) fitted onto an Axio Observer 7 fluorescence microscope (Carl Zeiss Microscopy LLC) with the 63x oil objective with a numerical aperture of 1.4 at room temperature. The following antibodies were used for immunofluorescence analysis: PDGFRα (1:100; RB-1691; Thermo Fisher Scientific); PDGFRβ (1:25; 28D4; 558820; BD, Franklin Lakes, NJ, USA); Na^+/K^+-ATPase (1:500; EP1845Y; ab76020; Abcam); Rab5 (1:200; C8B1; 3547; Cell Signaling Technology Inc.); Rab7 (1:100; D95F2; 9367; Cell Signaling Technology Inc.); Rab4 (1:200; ab13252; Abcam); Rab11 (1:100; D4F5; 5589; Cell Signaling Technology Inc.). For characterization of Venus expression in the absence of photobleaching, one independent trial, or biological replicate, was performed for each cell line, with at least 20 technical replicates consisting of individual cells imaged with Z-stacks (0.24 μm between Z-stacks with a range of 3-14 Z-stacks). For fluorescence intensity measurements, three independent trials, or biological replicates, were performed for each cell line. For each biological replicate, at least 40 technical replicates consisting of individual cells were imaged with Z-stacks (0.24 μm between Z-stacks with a range of 3-15 Z-stacks). For marker co-localization experiments, three independent trials, or biological replicates, were performed for each cell line. For each biological replicate, at least 20 technical replicates consisting of individual cells were imaged with Z-stacks (0.24 μm between Z-stacks with a range of 1-15 Z-

stacks) per timepoint. Images were deconvoluted using ZEN Blue software (Carl Zeiss Microscopy LLC) using the “Better, fast (Regularized Inverse Filter)” setting. For all images, extended depth of focus was applied to Z-stacks using ZEN Blue software (Carl Zeiss Microscopy LLC) to generate images with the maximum depth of field. For fluorescence intensity measurements, background was subtracted using rolling background subtraction with a radius of 30 pixels using Fiji software (version 2.1.0/1.53c; National Institutes of Health). A region of interest (ROI) was drawn around each Venus-positive cell, and integrated density was measured and recorded as the fluorescence intensity. For marker co-localization measurements, an ROI was drawn around each Venus-positive cell in the corresponding Cy3 (marker) channel using Fiji software (version 2.1.0/1.53c; National Institutes of Health). For each image with a given ROI, the Cy3 channel and the EGFP channel were converted to 8-bit images. Co-localization was measured using the Colocalization Threshold function, where the rcoloc value (Pearson’s correlation coefficient (PCC)) was used in statistical analysis. Statistical analyses were performed on the average values from each biological replicate with Prism 9 (GraphPad Software Inc.) using a two-tailed, unpaired *t*-test with Welch’s correction.

For Ki67 immunofluorescence experiments, cells were seeded onto glass coverslips coated with 5 μg/mL human plasma fibronectin purified protein (MilliporeSigma) at a density of 40,000 cells in RPMI growth medium. 24 h later, cells were washed with 1x phosphate buffered saline (PBS) and serum starved in HITES medium. HITES medium was replaced 23 h later and 1 h later cells were treated with 10 ng/mL PDGF-AA or PDGF-BB ligand (R&D Systems). After 24 h, cells were fixed in 4% paraformaldehyde (PFA) in PBS with 0.1% Triton X-100 for 10 min and washed in PBS with 0.1% Triton X-100. Cells were blocked for 1 h in 5% normal donkey serum (Jackson ImmunoResearch Inc.) in PBS and incubated overnight at 4ºC in Ki67 primary antibody (PA1-38032; Invitrogen) diluted 1:300 in 1% normal donkey serum in PBS. After washing in PBS, cells were incubated in Alexa Fluor 546-conjugated donkey anti-rabbit secondary antibody (1:1,000; A21206; Invitrogen) diluted in 1% normal donkey serum in PBS with 2 μg/mL DAPI (Sigma-Aldrich) for 1 h. Cells were mounted in VECTASHIELD HardSet Antifade Mounting Medium (Vector Laboratories, Inc.) and photographed using an Axiocam 506 mono digital camera (Carl Zeiss Microscopy LLC) fitted onto an Axio Observer 7 fluorescence microscope (Carl Zeiss Microscopy LLC) with the 20x air objective with a numerical aperture of 0.8 at room temperature. Three independent trials, or biological replicates, were performed for each cell line. For each biological replicate, 10 technical replicates consisting of individual fields of cells were imaged. All Ki67-positive signals were

confirmed by DAPI staining. Statistical analyses were performed on the average values from each biological replicate with Prism 9 (GraphPad Software Inc.) using a paired *t*-test within each cell line and a two-tailed, unpaired *t*-test with Welch's correction between each cell line.

HEK 293T/17 transient transfections

HEK 293T/17 cells were cultured in DMEM growth medium [DMEM (Gibco) supplemented with 100 U/mL penicillin (Gibco), 100 μg/mL streptomycin (Gibco) containing 10% FBS (Hyclone Laboratories Inc.)] at 37ºC in 5% carbon dioxide. Passage 20 cells at 70% confluence were transfected with pDEST-PDGFR-V1 and/or pDEST-PDGFR-V2 constructs (2.5 ug each) using Lipofectamine LTX (Thermo Fisher Scientific). Whole cell protein lysates were collected 24 h following transfection by resuspending cells in ice-cold NP-40 lysis buffer as detailed above.

Anchorage-independent growth assays

For measurement of anchorage-independent cell growth, 25,000 cells were suspended in 1.5 mL RPMI containing 100 U/mL penicillin (Gibco), 100 μg/mL streptomycin (Gibco), 10% FBS (Hyclone Laboratories Inc.) and 0.35% Difco Agar Noble (BD) and overlaid on a base layer containing 1.5 mL RPMI containing 100 U/mL penicillin (Gibco), 100 μg/mL streptomycin (Gibco), 10% FBS (Hyclone Laboratories Inc.) and 0.5% Difco Agar Noble (BD) in 6-well plates. A feeding layer of 2 mL RPMI growth medium supplemented with 10 ng/mL PDGF-AA or PDGF-BB ligand (R&D Systems) was added on top of the agar and replaced every day. Plates were incubated at 37ºC in 5% carbon dioxide for 10 days, and viable colonies were stained overnight with 1 mg/mL Nitrotetrazoleum Blue (Sigma-Aldrich) in PBS at 37ºC. Following a second overnight incubation at 4ºC, duplicate wells from each independent trial were photographed using a COOLPIX S600 digital camera (Nikon Inc., Melville, NY, USA). Images were made binary using Adobe Photoshop (version 21.0.3; Adobe Inc., San Jose, CA, USA), and colony number and area were quantified using Meta-Morph imaging software (Molecular Devices, LLC, San Jose, CA, USA). Statistical analyses were performed on average values from each of three biological replicates with Prism 9 (GraphPad Software Inc.) using a paired *t*-test within each cell line and a two-tailed, unpaired *t*-test with Welch's correction between each cell line.

Transwell assays

HCC15 cells were serum starved for 24 h in HITES medium. Cell culture inserts for 24-well plates containing polyethylene terephthalate membranes with 8 μm pores (Corning) were coated with 5 μg/mL human plasma fibronectin purified protein (MilliporeSigma). HCC15 cells were seeded at a density of 315,000 cells per insert in HITES medium and primary mouse embryonic palatal mesenchyme (MEPM) cells (see below) were seeded at a density of 250,000 cells per insert in DMEM starvation medium [DMEM (Gibco) supplemented with 100 U/mL penicillin (Gibco), 100 μg/mL streptomycin (Gibco) containing 0.1% FBS (Hyclone Laboratories Inc.)]. Inserts with HCC15 cells were immersed in 500 µL RPMI growth medium and inserts with MEPM cells were immersed in 500 µL DMEM growth medium in the absence or presence of 10 ng/mL PDGF-AA or PDGF-BB ligand (R&D Systems) for 24 h. Migrated cells were subsequently fixed in 4% PFA in PBS for 10 min and stained in 0.1% crystal violet in 10% ethanol for 10 min. Dried inserts were photographed using an Axiocam 105 color camera fitted onto a Stemi 508 stereo microscope at 25x magnification at room temperature (Carl Zeiss Microscopy LLC). Five fields of cells from each independent trial were photographed and quantified by measuring integrated density with ImageJ software (version 1.52a; National Institutes of Health). For MEPM cells, independent trials consisted of cells derived from a single conditional knockout embryo or pooled cells from two conditional knockout littermates. Statistical analyses were performed on average values from each of six (HCC15 cells) or three (MEPM cells) biological replicates with Prism 9 (GraphPad Software Inc.) using a paired *t*-test within each cell line and a two-tailed, unpaired *t*-test with Welch's correction between each cell line.

Mouse strains and primary MEPM culture

All animal experimentation was approved by the Institutional Animal Care and Use Committee of the University of Colorado Anschutz Medical Campus. *Pdgfra*^{tm8Sor} mice (Tallquist and Soriano, 2003), referred to in the text as *Pdgfra*^{fl}; *Pdgfrb*^{tm11Sor} mice (Schmahl et al., 2008), referred to in the text as *Pdgfrb*^{fl}; and *H2az2*$^{Tg(Wnt1\text{-}cre)11Rth}$ mice (Danielian et al., 1998), referred to in the text as *Wnt1-Cre*^{Tg}, were maintained on a 129S4 coisogenic genetic background and housed at a sub-thermoneutral temperature of 21-23ºC. Mice were euthanized by inhalation of carbon dioxide from compressed gas. Cervical dislocation was used as a secondary verification of death. Both male and female embryos were analyzed. Primary mouse embryonic palatal mesenchyme (MEPM) cells were isolated from the palatal

shelves of embryos dissected at embryonic day 13.5 in PBS and cultured in DMEM growth medium at 37ºC in 5% carbon dioxide.

Crystal violet growth assays

11,500 passage 2 MEPM cells were seeded into wells of a 24-well plate and cultured in DMEM growth medium. After 24 h, medium was aspirated and replaced with fresh DMEM growth medium or DMEM starvation medium. After 24 h, cells were stimulated with 10 ng/mL PDGF-AA or PDGF-BB ligand (R&D Systems). Cells were fixed after 24 h in 4% PFA in PBS, stained with 0.1% crystal violet in 10% ethanol, extracted with 10% acetic acid, and the absorbance measured at 590 nm. Three independent trials were performed, each consisting of MEPM cells derived from a single conditional knockout embryo or non-pooled cells from two conditional knockout littermates. Statistical analyses were performed on individual values with Prism 9 (GraphPad Software Inc.) using a two-tailed, unpaired *t*-test with Welch's correction.

Acknowledgements

We thank Julia Mo, Damian Garno and Jessica Johnston for technical assistance. Cell sorting was performed at the University of Colorado Cancer Center Flow Cytometry Shared Resource (Cancer Center Support Grant P30CA046934). We are grateful to the laboratory of Dr. Rytis Prekeris for lentiviral and packaging plasmids and the laboratory of Dr. Lynn Heasley for HCC15 cells. We thank members of the Fantauzzo laboratory and Dr. Rytis Prekeris for their critical comments on the manuscript.

Competing interests

No competing interests declared.

Author contributions

Conceptualization, K.A.F. and M.A.R.; Methodology, M.A.R. and K.A.F.; Formal analysis, M.A.R.; Investigation, M.A.R., M.B.C., R.L. and K.A.F.; Writing – original draft, M.A.R.; Writing – review & editing, M.A.R., M.B.C. and K.A.F.; Visualization, M.A.R. and K.A.F.; Supervision, K.A.F.; Funding acquisition, M.A.R. and K.A.F.

Funding

This work was supported by the National Institutes of Health [R01DE027689 to K.A.F., K02DE028572 to K.A.F. and F31DE029976 to M.A.R.].

References

Bae, J. H. and Schlessinger, J. (2010). Asymmetric tyrosine kinase arrangements in activation or autophosphorylation of receptor tyrosine kinases. *Mol Cells* **29**, 443-8.

Bagchi, S., Fredriksson, R. and Wallen-Mackenzie, A. (2015). In Situ Proximity Ligation Assay (PLA). *Methods Mol Biol* **1318**, 149-59.

Barretina, J., Caponigro, G., Stransky, N., Venkatesan, K., Margolin, A. A., Kim, S., Wilson, C. J., Lehar, J., Kryukov, G. V., Sonkin, D. et al. (2012). The Cancer Cell Line Encyclopedia enables predictive modelling of anticancer drug sensitivity. *Nature* **483**, 603-7.

Bonifacino, J. S. and Traub, L. M. (2003). Signals for sorting of transmembrane proteins to endosomes and lysosomes. *Annu Rev Biochem* **72**, 395-447.

Bostrom, H., Willetts, K., Pekny, M., Leveen, P., Lindahl, P., Hedstrand, H., Pekna, M., Hellstrom, M., GebreMedhin, S., Schalling, M. et al. (1996). PDGF-A signaling is a critical event in lung alveolar myofibroblast development and alveogenesis. *Cell* **85**, 863-873.

Bouyain, S., Longo, P. A., Li, S., Ferguson, K. M. and Leahy, D. J. (2005). The extracellular region of ErbB4 adopts a tethered conformation in the absence of ligand. *Proc Natl Acad Sci U S A* **102**, 15024-9.

Bruggemann, Y., Karajannis, L. S., Stanoev, A., Stallaert, W. and Bastiaens, P. I. H. (2021). Growth factor-dependent ErbB vesicular dynamics couple receptor signaling to spatially and functionally distinct Erk pools. *Sci Signal* **14**.

Cancer Cell Line Encyclopedia, C. and Genomics of Drug Sensitivity in Cancer, C. (2015). Pharmacogenomic agreement between two cancer cell line data sets. *Nature* **528**, 84-7.

Chen, P. H., Unger, V. and He, X. (2015). Structure of Full-Length Human PDGFRbeta Bound to Its Activating Ligand PDGF-B as Determined by Negative-Stain Electron Microscopy. *J Mol Biol* **427**, 3921-34.

Chiara, F., Bishayee, S., Heldin, C. H. and Demoulin, J. B. (2004). Autoinhibition of the platelet-derived growth factor beta-receptor tyrosine kinase by its C-terminal tail. *J Biol Chem* **279**, 19732-8.

Cho, H. S. and Leahy, D. J. (2002). Structure of the extracellular region of HER3 reveals an interdomain tether. *Science* **297**, 1330-3.

Cho, H. S., Mason, K., Ramyar, K. X., Stanley, A. M., Gabelli, S. B., Denney, D. W., Jr. and Leahy, D. J. (2003). Structure of the extracellular region of HER2 alone and in complex with the Herceptin Fab. *Nature* **421**, 756-60.

Croucher, D. R., Iconomou, M., Hastings, J. F., Kennedy, S. P., Han, J. Z., Shearer, R. F., McKenna, J., Wan, A., Lau, J., Aparicio, S. et al. (2016). Bimolecular complementation affinity purification (BiCAP) reveals dimer-specific protein interactions for ERBB2 dimers. *Sci Signal* **9**, ra69.

Danielian, P. S., Muccino, D., Rowitch, D. H., Michael, S. K. and McMahon, A. P. (1998). Modification of gene activity in mouse embryos in utero by a tamoxifen-inducible form of Cre recombinase. *Curr Biol* **8**, 1323-6.

De Donatis, A., Comito, G., Buricchi, F., Vinci, M. C., Parenti, A., Caselli, A., Camici, G., Manao, G., Ramponi, G. and Cirri, P. (2008). Proliferation versus migration in platelet-derived growth factor signaling: the key role of endocytosis. *J Biol Chem* **283**, 19948-56.

Ding, H., Wu, X., Bostrom, H., Kim, I., Wong, N., Tsoi, B., O'Rourke, M., Koh, G. Y., Soriano, P., Betsholtz, C. et al. (2004). A specific requirement for PDGF-C in palate formation and PDGFR-alpha signaling. *Nat Genet* **36**, 1111-6.

Disanza, A., Frittoli, E., Palamidessi, A. and Scita, G. (2009). Endocytosis and spatial restriction of cell signaling. *Mol Oncol* **3**, 280-96.

Ekman, S., Thuresson, E. R., Heldin, C. H. and Ronnstrand, L. (1999). Increased mitogenicity of an alphabeta heterodimeric PDGF receptor complex correlates with lack of RasGAP binding. *Oncogene* **18**, 2481-8.

Fantauzzo, K. A. and Soriano, P. (2015). Receptor tyrosine kinase signaling: regulating neural crest development one phosphate at a time. *Curr Top Dev Biol* **111**, 135-82.

Fantauzzo, K. A. and Soriano, P. (2016). PDGFRbeta regulates craniofacial development through homodimers and functional heterodimers with PDGFRalpha. *Genes Dev* **30**, 2443-2458.

Ferguson, K. M., Berger, M. B., Mendrola, J. M., Cho, H. S., Leahy, D. J. and Lemmon, M. A. (2003). EGF activates its receptor by removing interactions that autoinhibit ectodomain dimerization. *Mol Cell* **11**, 507-17.

Freed, D. M., Bessman, N. J., Kiyatkin, A., Salazar-Cavazos, E., Byrne, P. O., Moore, J. O., Valley, C. C., Ferguson, K. M., Leahy, D. J., Lidke, D. S. et al. (2017). EGFR Ligands Differentially Stabilize Receptor Dimers to Specify Signaling Kinetics. *Cell* **171**, 683-695 e18.

Garrett, T. P., McKern, N. M., Lou, M., Elleman, T. C., Adams, T. E., Lovrecz, G. O., Kofler, M., Jorissen, R. N., Nice, E. C., Burgess, A. W. et al. (2003). The crystal structure of a truncated ErbB2 ectodomain reveals an active conformation, poised to interact with other ErbB receptors. *Mol Cell* **11**, 495-505.

Gerdes, J., Lemke, H., Baisch, H., Wacker, H. H., Schwab, U. and Stein, H. (1984). Cell cycle analysis of a cell proliferation-associated human nuclear antigen defined by the monoclonal antibody Ki-67. *J Immunol* **133**, 1710-5.

Heldin, C. H. and Westermark, B. (1999). Mechanism of action and in vivo role of platelet-derived growth factor. *Physiol Rev* **79**, 1283-316.

Hellberg, C., Schmees, C., Karlsson, S., Ahgren, A. and Heldin, C. H. (2009). Activation of protein kinase C alpha is necessary for sorting the PDGF beta-receptor to Rab4a-dependent recycling. *Molecular Biology of the Cell* **20**, 2856-63.

Herren, B., Rooney, B., Weyer, K. A., Iberg, N., Schmid, G. and Pech, M. (1993). Dimerization of extracellular domains of platelet-derived growth factor receptors. A revised model of receptor-ligand interaction. *J Biol Chem* **268**, 15088-95.

Herrero, A., Casar, B., Colon-Bolea, P., Agudo-Ibanez, L. and Crespo, P. (2016). Defined spatiotemporal features of RAS-ERK signals dictate cell fate in MCF-7 mammary epithelial cells. *Molecular Biology of the Cell* **27**, 1958-68.

Hoch, R. V. and Soriano, P. (2003). Roles of PDGF in animal development. *Development* **130**, 4769-84.

Hu, C. D. and Kerppola, T. K. (2003). Simultaneous visualization of multiple protein interactions in living cells using multicolor fluorescence complementation analysis. *Nature Biotechnology* **21**, 539-545.

Jastrzebski, K., Zdzalik-Bielecka, D., Maminska, A., Kalaidzidis, Y., Hellberg, C. and Miaczynska, M. (2017). Multiple routes of endocytic internalization of PDGFRbeta contribute to PDGF-induced STAT3 signaling. *J Cell Sci* **130**, 577-589.

Karlsson, S., Kowanetz, K., Sandin, A., Persson, C., Ostman, A., Heldin, C. H. and Hellberg, C. (2006). Loss of T-cell protein tyrosine phosphatase induces recycling of the platelet-derived growth factor (PDGF) beta-receptor but not the PDGF alpha-receptor. *Molecular Biology of the Cell* **17**, 4846-55.

Kelly, J. D., Haldeman, B. A., Grant, F. J., Murray, M. J., Seifert, R. A., Bowen-Pope, D. F., Cooper, J. A. and Kazlauskas, A. (1991). Platelet-derived growth factor (PDGF) stimulates PDGF receptor subunit dimerization and intersubunit trans-phosphorylation. *J Biol Chem* **266**, 8987-92.

Keyes, J., Ganesan, A., Molinar-Inglis, O., Hamidzadeh, A., Zhang, J., Ling, M., Trejo, J., Levchenko, A. and Zhang, J. (2020). Signaling diversity enabled by Rap1-regulated plasma membrane ERK with distinct temporal dynamics. *Elife* **9**.

Klinghoffer, R. A., Hamilton, T. G., Hoch, R. and Soriano, P. (2002). An allelic series at the PDGFalphaR locus indicates unequal contributions of distinct signaling pathways during development. *Dev Cell* **2**, 103-13.

Klinghoffer, R. A., Mueting-Nelsen, P. F., Faerman, A., Shani, M. and Soriano, P. (2001). The two PDGF receptors maintain conserved signaling in vivo despite divergent embryological functions. *Mol Cell* **7**, 343-54.

Lemmon, M. A. and Schlessinger, J. (2010). Cell signaling by receptor tyrosine kinases. *Cell* **141**, 1117-34.

Leveen, P., Pekny, M., Gebremedhin, S., Swolin, B., Larsson, E. and Betsholtz, C. (1994). Mice Deficient for Pdgf-B Show Renal, Cardiovascular, and Hematological Abnormalities. *Genes & Development* **8**, 1875-1887.

Li, X., Ba, Q., Liu, Y., Yue, Q., Chen, P., Li, J., Zhang, H., Ying, H., Ding, Q., Song, H. et al. (2017). Dihydroartemisinin selectively inhibits PDGFRalpha-positive ovarian cancer growth and metastasis through inducing degradation of PDGFRalpha protein. *Cell Discov* **3**, 17042.

Magliery, T. J., Wilson, C. G., Pan, W., Mishler, D., Ghosh, I., Hamilton, A. D. and Regan, L. (2005). Detecting protein-protein interactions with a green fluorescent protein fragment reassembly trap: scope and mechanism. *J Am Chem Soc* **127**, 146-57.

Marshall, C. J. (1995). Specificity of receptor tyrosine kinase signaling: transient versus sustained extracellular signal-regulated kinase activation. *Cell* **80**, 179-85.

Matsui, T., Heidaran, M., Miki, T., Popescu, N., La Rochelle, W., Kraus, M., Pierce, J. and Aaronson, S. (1989). Isolation of a novel receptor cDNA establishes the existence of two PDGF receptor genes. *Science* **243**, 800-4.

McCluskey, A., Daniel, J. A., Hadzic, G., Chau, N., Clayton, E. L., Mariana, A., Whiting, A., Gorgani, N. N., Lloyd, J., Quan, A. et al. (2013). Building a better dynasore: the dyngo compounds potently inhibit dynamin and endocytosis. *Traffic* **14**, 1272-89.

Mellman, I. (1996). Endocytosis and molecular sorting. *Annu Rev Cell Dev Biol* **12**, 575-625.

Miaczynska, M. (2013). Effects of membrane trafficking on signaling by receptor tyrosine kinases. *Cold Spring Harb Perspect Biol* **5**, a009035.

Miyake, S., Lupher, M. L., Jr., Druker, B. and Band, H. (1998). The tyrosine kinase regulator Cbl enhances the ubiquitination and degradation of the platelet-derived growth factor receptor alpha. *Proc Natl Acad Sci U S A* **95**, 7927-32.

Miyake, S., Mullane-Robinson, K. P., Lill, N. L., Douillard, P. and Band, H. (1999). Cbl-mediated negative regulation of platelet-derived growth factor receptor-dependent cell proliferation. A critical role for Cbl tyrosine kinase-binding domain. *J Biol Chem* **274**, 16619-28.

Mo, J., Long, R. and Fantauzzo, K. A. (2020). Pdgfra and Pdgfrb Genetically Interact in the Murine Neural Crest Cell Lineage to Regulate Migration and Proliferation. *Front Physiol* **11**, 588901.

Mori, S., Claesson-Welsh, L. and Heldin, C. H. (1991). Identification of a hydrophobic region in the carboxyl terminus of the platelet-derived growth factor beta-receptor which is important for ligand-mediated endocytosis. *J Biol Chem* **266**, 21158-64.

Mori, S., Tanaka, K., Omura, S. and Saito, Y. (1995). Degradation process of ligand-stimulated platelet-derived growth factor beta-receptor involves ubiquitin-proteasome proteolytic pathway. *J Biol Chem* **270**, 29447-52.

Pahara, J., Shi, H., Chen, X. and Wang, Z. (2010). Dimerization drives PDGF receptor endocytosis through a C-terminal hydrophobic motif shared by EGF receptor. *Exp Cell Res* **316**, 2237-50.

Polyansky, A. A., Bocharov, E. V., Velghe, A. I., Kuznetsov, A. S., Bocharova, O. V., Urban, A. S., Arseniev, A. S., Zagrovic, B., Demoulin, J. B. and Efremov, R. G. (2019). Atomistic mechanism of the constitutive activation of PDGFRA via its transmembrane domain. *Biochim Biophys Acta Gen Subj* **1863**, 82-95.

Reddi, A. L., Ying, G., Duan, L., Chen, G., Dimri, M., Douillard, P., Druker, B. J., Naramura, M., Band, V. and Band, H. (2007). Binding of Cbl to a phospholipase Cgamma1-docking site on platelet-derived growth factor receptor beta provides a dual mechanism of negative regulation. *J Biol Chem* **282**, 29336-47.

Rogers, M. A. and Fantauzzo, K. A. (2020). The emerging complexity of PDGFRs: activation, internalization and signal attenuation. *Biochem Soc Trans* **48**, 1167-1176.

Rorsman, C., Tsioumpekou, M., Heldin, C. H. and Lennartsson, J. (2016). The Ubiquitin Ligases c-Cbl and Cbl-b Negatively Regulate Platelet-derived Growth Factor (PDGF) BB-induced Chemotaxis by Affecting PDGF Receptor beta (PDGFRbeta) Internalization and Signaling. *J Biol Chem* **291**, 11608-18.

Sadowski, L., Jastrzebski, K., Kalaidzidis, Y., Heldin, C. H., Hellberg, C. and Miaczynska, M. (2013). Dynamin inhibitors impair endocytosis and mitogenic signaling of PDGF. *Traffic* **14**, 725-36.

Schlessinger, J. (2000). Cell signaling by receptor tyrosine kinases. *Cell* **103**, 211-25.

Schmahl, J., Rizzolo, K. and Soriano, P. (2008). The PDGF signaling pathway controls multiple steroid-producing lineages. *Genes Dev* **22**, 3255-67.

Schmid, F. M., Schou, K. B., Vilhelm, M. J., Holm, M. S., Breslin, L., Farinelli, P., Larsen, L. A., Andersen, J. S., Pedersen, L. B. and Christensen, S. T. (2018). IFT20 modulates ciliary PDGFRalpha signaling by regulating the stability of Cbl E3 ubiquitin ligases. *J Cell Biol* **217**, 151-161.

Seifert, R. A., Hart, C. E., Phillips, P. E., Forstrom, J. W., Ross, R., Murray, M. J. and Bowen-Pope, D. F. (1989). Two different subunits associate to create isoform-specific platelet-derived growth factor receptors. *J Biol Chem* **264**, 8771-8.

Shim, A. H., Liu, H., Focia, P. J., Chen, X., Lin, P. C. and He, X. (2010). Structures of a platelet-derived growth factor/propeptide complex and a platelet-derived growth factor/receptor complex. *Proc Natl Acad Sci U S A* **107**, 11307-12.

Skou, J. C. (1989). The identification of the sodium-pump as the membrane-bound Na+/K+-ATPase: a commentary on 'The Influence of Some Cations on an Adenosine Triphosphatase from Peripheral Nerves'. *Biochim Biophys Acta* **1000**, 435-8.

Soriano, P. (1994). Abnormal kidney development and hematological disorders in PDGF beta-receptor mutant mice. *Genes Dev* **8**, 1888-96.
Soriano, P. (1997). The PDGF alpha receptor is required for neural crest cell development and for normal patterning of the somites. *Development* **124**, 2691-700.
Sparta, B., Pargett, M., Minguet, M., Distor, K., Bell, G. and Albeck, J. G. (2015). Receptor Level Mechanisms Are Required for Epidermal Growth Factor (EGF)-stimulated Extracellular Signal-regulated Kinase (ERK) Activity Pulses. *J Biol Chem* **290**, 24784-92.
Stewart, S. A., Dykxhoorn, D. M., Palliser, D., Mizuno, H., Yu, E. Y., An, D. S., Sabatini, D. M., Chen, I. S., Hahn, W. C., Sharp, P. A. et al. (2003). Lentivirus-delivered stable gene silencing by RNAi in primary cells. *RNA* **9**, 493-501.
Tallquist, M. D. and Soriano, P. (2003). Cell autonomous requirement for PDGFRalpha in populations of cranial and cardiac neural crest cells. *Development* **130**, 507-18.
Teis, D., Wunderlich, W. and Huber, L. A. (2002). Localization of the MP1-MAPK scaffold complex to endosomes is mediated by p14 and required for signal transduction. *Dev Cell* **3**, 803-14.
Vasudevan, H. N., Mazot, P., He, F. and Soriano, P. (2015). Receptor tyrosine kinases modulate distinct transcriptional programs by differential usage of intracellular pathways. *Elife* **4**.
Wang, Y., Pennock, S. D., Chen, X., Kazlauskas, A. and Wang, Z. (2004). Platelet-derived growth factor receptor-mediated signal transduction from endosomes. *J Biol Chem* **279**, 8038-46.
Wiesmann, U. N., DiDonato, S. and Herschkowitz, N. N. (1975). Effect of chloroquine on cultured fibroblasts: release of lysosomal hydrolases and inhibition of their uptake. *Biochem Biophys Res Commun* **66**, 1338-43.
Williams, L. T. (1989). Signal transduction by the platelet-derived growth factor receptor involves association of the receptor with cytoplasmic molecules. *Clin Res* **37**, 564-8.
Yang, Y., Xie, P., Opatowsky, Y. and Schlessinger, J. (2010). Direct contacts between extracellular membrane-proximal domains are required for VEGF receptor activation and cell signaling. *Proc Natl Acad Sci U S A* **107**, 1906-11.
Zerial, M. and McBride, H. (2001). Rab proteins as membrane organizers (vol 2, pg 107, 2001). *Nature Reviews Molecular Cell Biology* **2**, 216-216.
Zhang, X., Gureasko, J., Shen, K., Cole, P. A. and Kuriyan, J. (2006). An allosteric mechanism for activation of the kinase domain of epidermal growth factor receptor. *Cell* **125**, 1137-49.
Zufferey, R., Nagy, D., Mandel, R. J., Naldini, L. and Trono, D. (1997). Multiply attenuated lentiviral vector achieves efficient gene delivery in vivo. *Nat Biotechnol* **15**, 871-5.

Figures

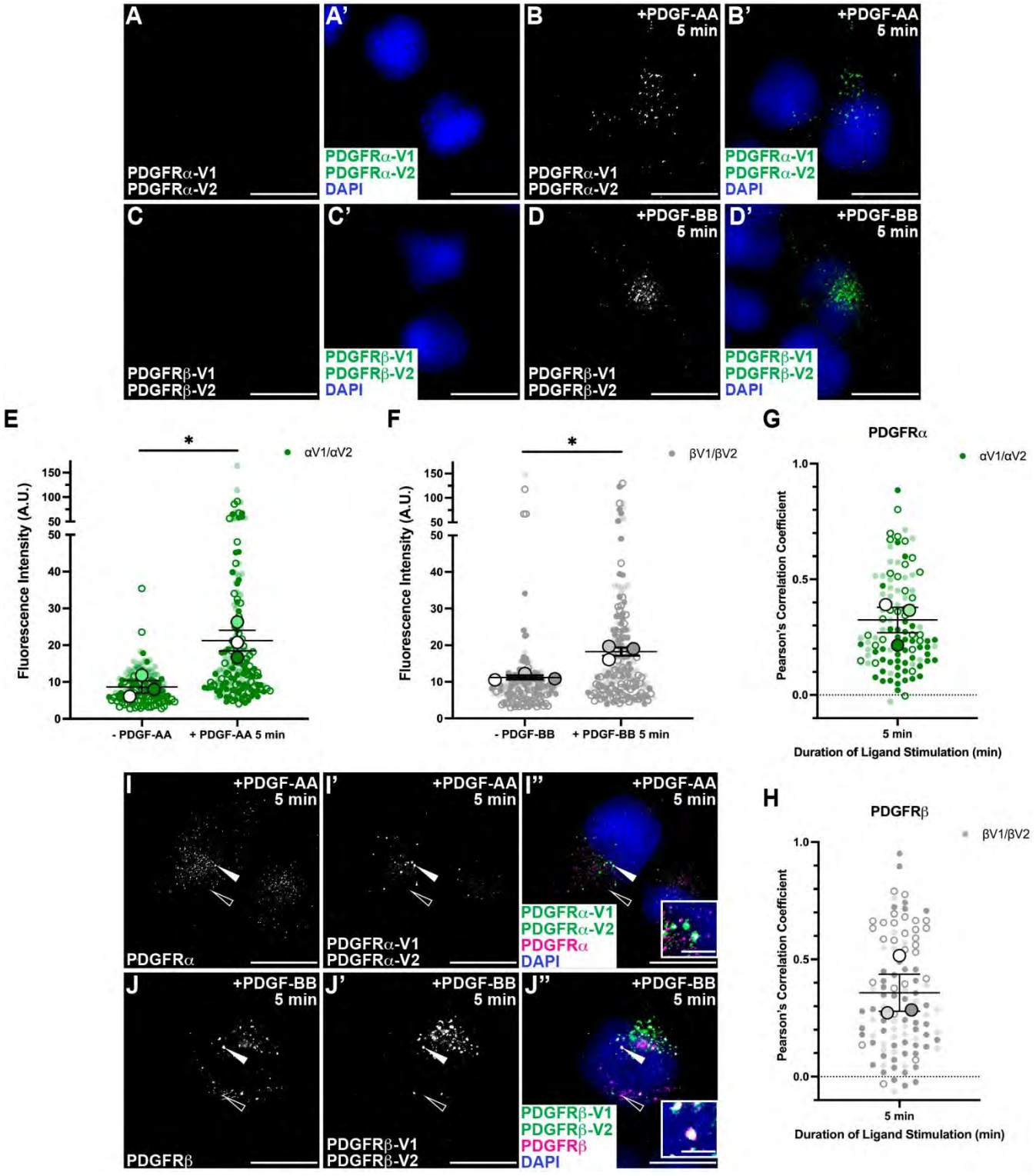

Fig. 1. Validation of PDGFR-BiFC stable cell lines. (A-D') Venus expression (white/green) as assessed by fluorescence analysis of HCC15 cells transduced with PDGFRα-V1 and PDGFRα-V2 (A-B') or PDGFRβ-V1 and PDGFRβ-V2 (C-D') in the absence (A,A',C,C') or presence (B,B',D,D') of PDGF ligand for 5 min. Nuclei were stained with DAPI (blue; A'-D'). Scale bars, 20 μm. (E,F) Scatter dot plots depicting fluorescence intensity for PDGFRα homodimer (E) and PDGFRβ homodimer (F) cell lines. Data are mean ± s.e.m. Statistical analyses were performed using a two-tailed, unpaired *t*-test with Welch's correction. *, $p<0.05$. Colored circles correspond to independent experiments. Summary statistics from biological replicates consisting of independent experiments are superimposed on top of data from all cells. $n>40$ technical replicates across each of 3 biological replicates. (G,H) Scatter dot plots depicting Pearson's correlation coefficient of PDGFRα homodimer cell line with an anti-PDGFRα antibody (G) and PDGFRβ homodimer cell line with an anti-PDGFRβ antibody (H) following PDGF ligand stimulation for 5 min. Data are mean ± s.e.m. Colored circles correspond to independent experiments. Summary statistics from biological replicates consisting of independent experiments are superimposed on top of data from all cells. $n>20$ technical replicates across each of 3 biological replicates. (I-J") PDGFR antibody expression (white/magenta; I,I",J,J") and/or Venus expression (white/green; I',I",J',J") as assessed by (immuno)fluorescence analysis of PDGFRα homodimer (I-I") and PDGFRβ homodimer (J-J") cell lines. Insets in I" and J" are regions where white arrows are pointing. Nuclei were stained with DAPI (blue; I",J"). White arrows denote co-localization; white outlined arrows denote lack of co-localization. Scale bars, 20 μm. Inset scale bars, 3 μm.

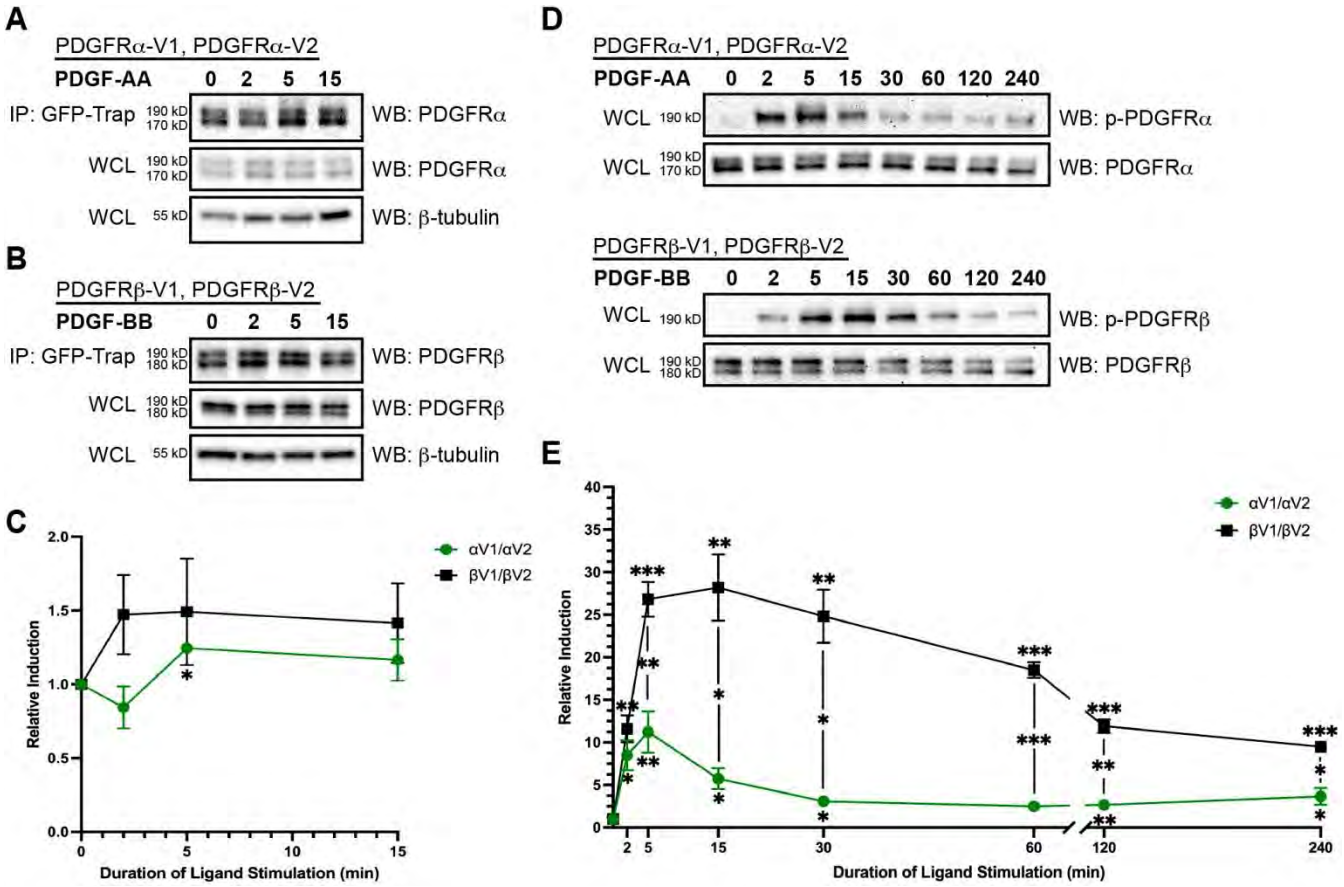

Fig. 2. PDGFRβ receptors homodimerize more quickly than PDGFRα receptors with increased levels of autophosphorylation. (A,B) Immunoprecipitation (IP) of dimerized PDGFRα receptors (A) and PDGFRβ receptors (B) with GFP-Trap nanobody from cells that were treated with PDGF ligand for 2-15 min followed by western blotting (WB) with anti-PDGFRα (A) or PDGFRβ (B) antibodies. (C) Line graph depicting quantification of band intensities from *n*=3 biological replicates as in A and B. Data are mean ± s.e.m. Statistical analyses were performed using a two-tailed, ratio paired *t*-test within each cell line and a two-tailed, unpaired *t*-test with Welch's correction between each cell line. *, p<0.05. (D) Western blot analysis of whole cell lysates (WCL) from PDGFRα homodimer (top) and PDGFRβ homodimer (bottom) cell lines following a timecourse of PDGF ligand stimulation from 2 min to 4 h with an anti-phospho-PDGFR antibody. (E) Line graph depicting quantification of band intensities from *n*=3 biological replicates as in D. Data are mean ± s.e.m. Statistical analyses were performed using a two-tailed, ratio paired *t*-test within each cell line and a two-tailed, unpaired *t*-test with Welch's correction between each cell line. *, p<0.05; **, p<0.01; ***, p<0.001.

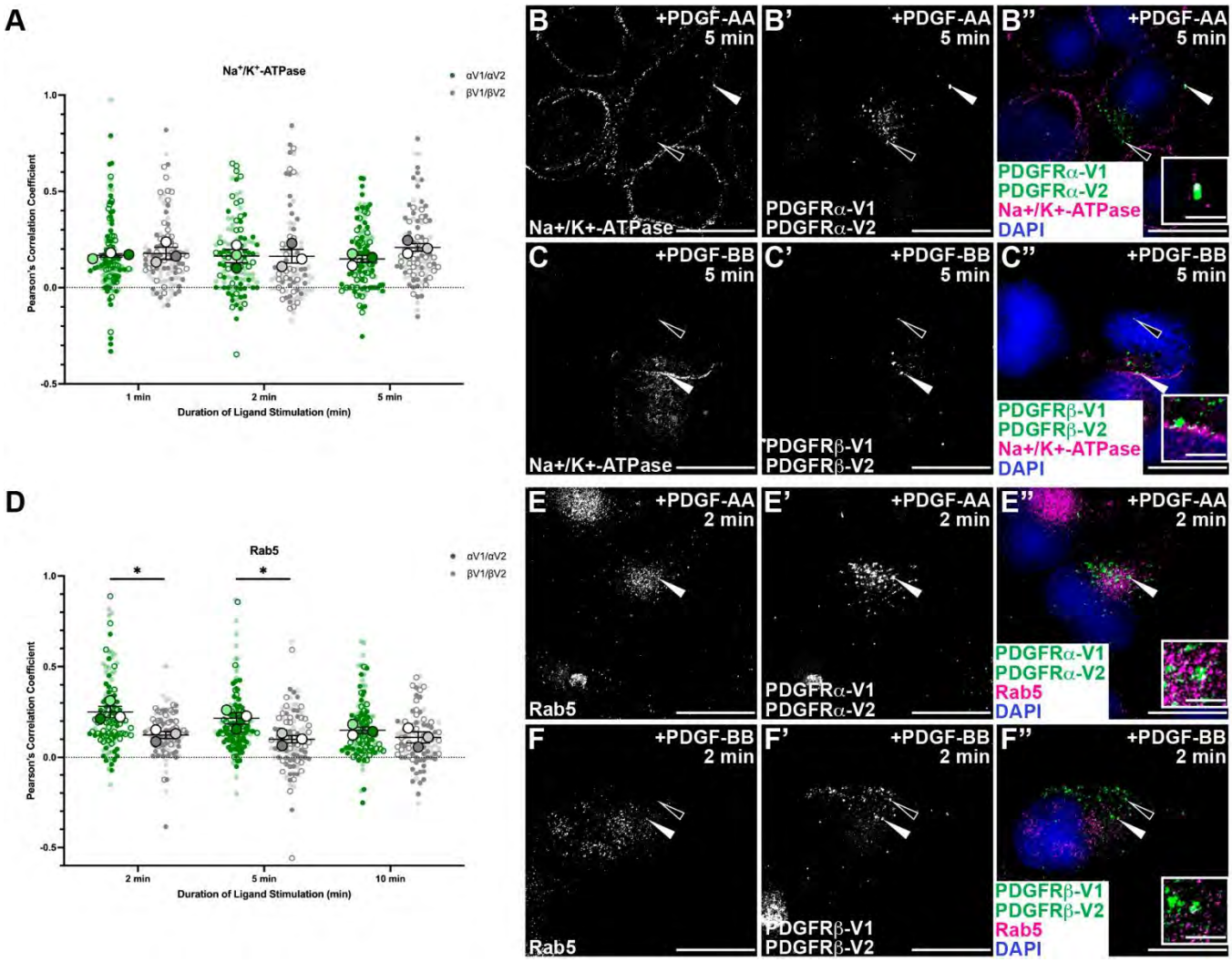

Fig. 3. PDGFRα homodimers are trafficked more quickly than PDGFRβ homodimers. (A,D) Scatter dot plots depicting Pearson's correlation coefficient of the PDGFRα homodimer and PDGFRβ homodimer cell lines with an anti-Na^+/K^+-ATPase antibody (A) or an anti-Rab5 antibody (D) following PDGF ligand stimulation from 1-5 min (A) or 2-10 min (D). Data are mean ± s.e.m. Statistical analyses were performed using a two-tailed, unpaired *t*-test with Welch's correction. *, $p<0.05$. Colored circles correspond to independent experiments. Summary statistics from biological replicates consisting of independent experiments are superimposed on top of data from all cells. *n*>20 technical replicates across each of 3 biological replicates. (B-C",E-F") Na^+/K^+-ATPase antibody expression (white/magenta; B,B",C,C") or Rab5 antibody expression (white/magenta; E,E",F,F") and/or Venus expression (white/green; B',B",C',C",E',E",F',F") as assessed by (immuno)fluorescence analysis of PDGFRα homodimer (B-B",E-E") and PDGFRβ homodimer (C-C",F-F") cell lines. Insets in B",

C”, E” and F’’ are regions where white arrows are pointing. Nuclei were stained with DAPI (blue; B”,C”,E”,F”). White arrows denote co-localization; white outlined arrows denote lack of co-localization. Scale bars, 20 μm. Inset scale bars, 3 μm.

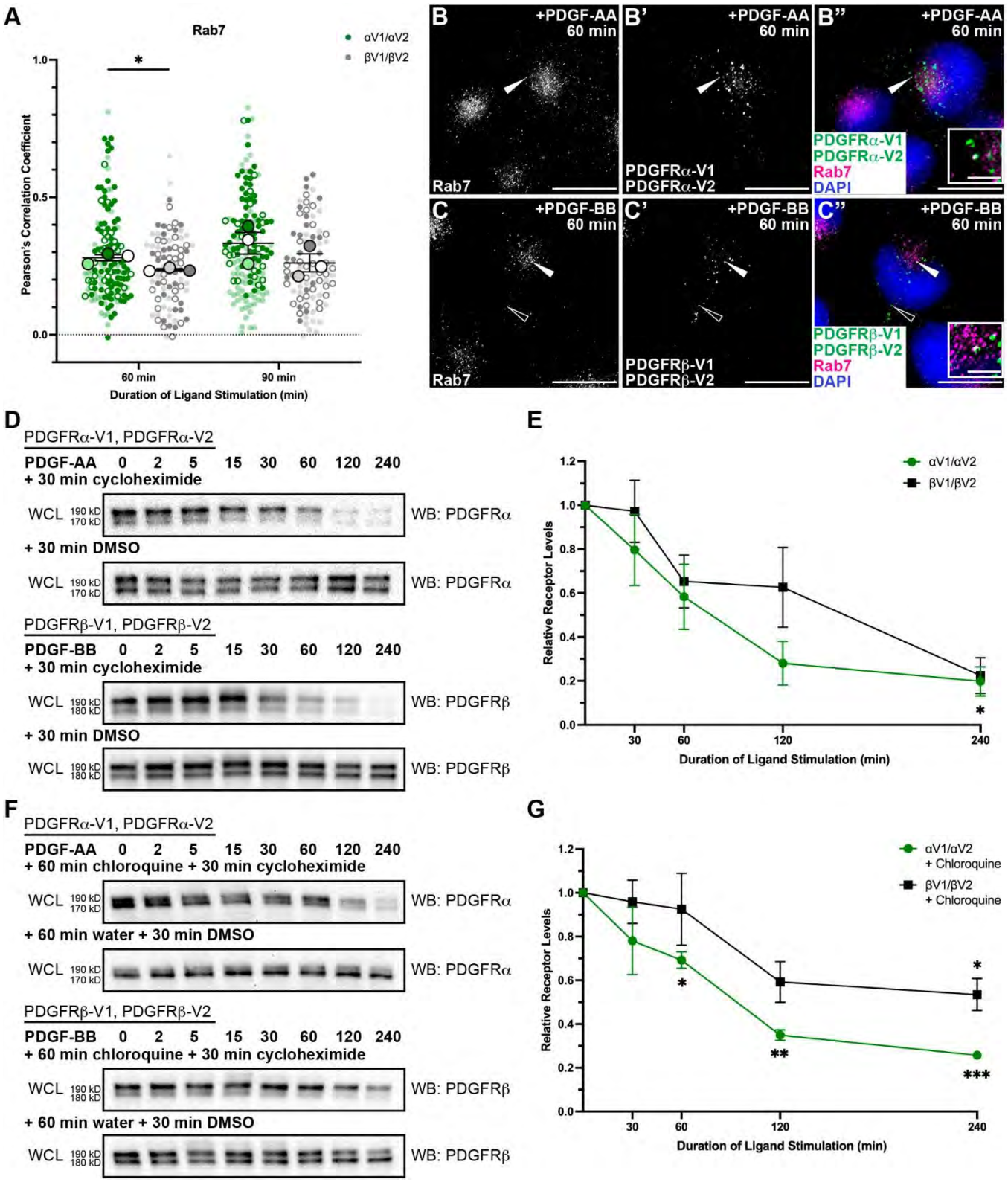

Fig. 4. PDGFRα homodimers are degraded more quickly than PDGFRβ homodimers.

(A) Scatter dot plot depicting Pearson's correlation coefficient of the PDGFRα homodimer and PDGFRβ homodimer cell lines with an anti-Rab7 antibody following PDGF ligand stimulation

from 60-90 min. Data are mean ± s.e.m. Statistical analyses were performed using a two-tailed, unpaired *t*-test with Welch's correction. *, p<0.05. Colored circles correspond to independent experiments. Summary statistics from biological replicates consisting of independent experiments are superimposed on top of data from all cells. *n*>20 technical replicates across each of 3 biological replicates. (B-C") Rab7 antibody expression (white/magenta; B,B",C,C") and/or Venus expression (white/green; B',B",C',C") as assessed by (immuno)fluorescence analysis of PDGFRα homodimer (B-B") and PDGFRβ homodimer (C-C") cell lines. Insets in B" and C" are regions where white arrows are pointing. Nuclei were stained with DAPI (blue; B",C"). White arrows denote co-localization; white outlined arrows denote lack of co-localization. Scale bars, 20 μm. Inset scale bars, 3 μm. (D,F) Western blot (WB) analysis of whole cell lysates (WCL) from PDGFRα homodimer (top) and PDGFRβ homodimer (bottom) cell lines following pretreatment with 10 μg/mL cycloheximide (D) or 25 μM chloroquine plus 10 μg/mL cycloheximide (F) and a timecourse of PDGF ligand stimulation from 2 min to 4 h with anti-PDGFRα (top) or anti-PDGFRβ (bottom) antibodies. (E,G) Line graphs depicting quantification of band intensities from *n*=3 biological replicates as in D and F. Data are mean ± s.e.m. Statistical analyses were performed using a two-tailed, ratio paired *t*-test within each cell line and a two-tailed, unpaired *t*-test with Welch's correction between each cell line. *, p<0.05; **, p<0.01; ***, p<0.001.

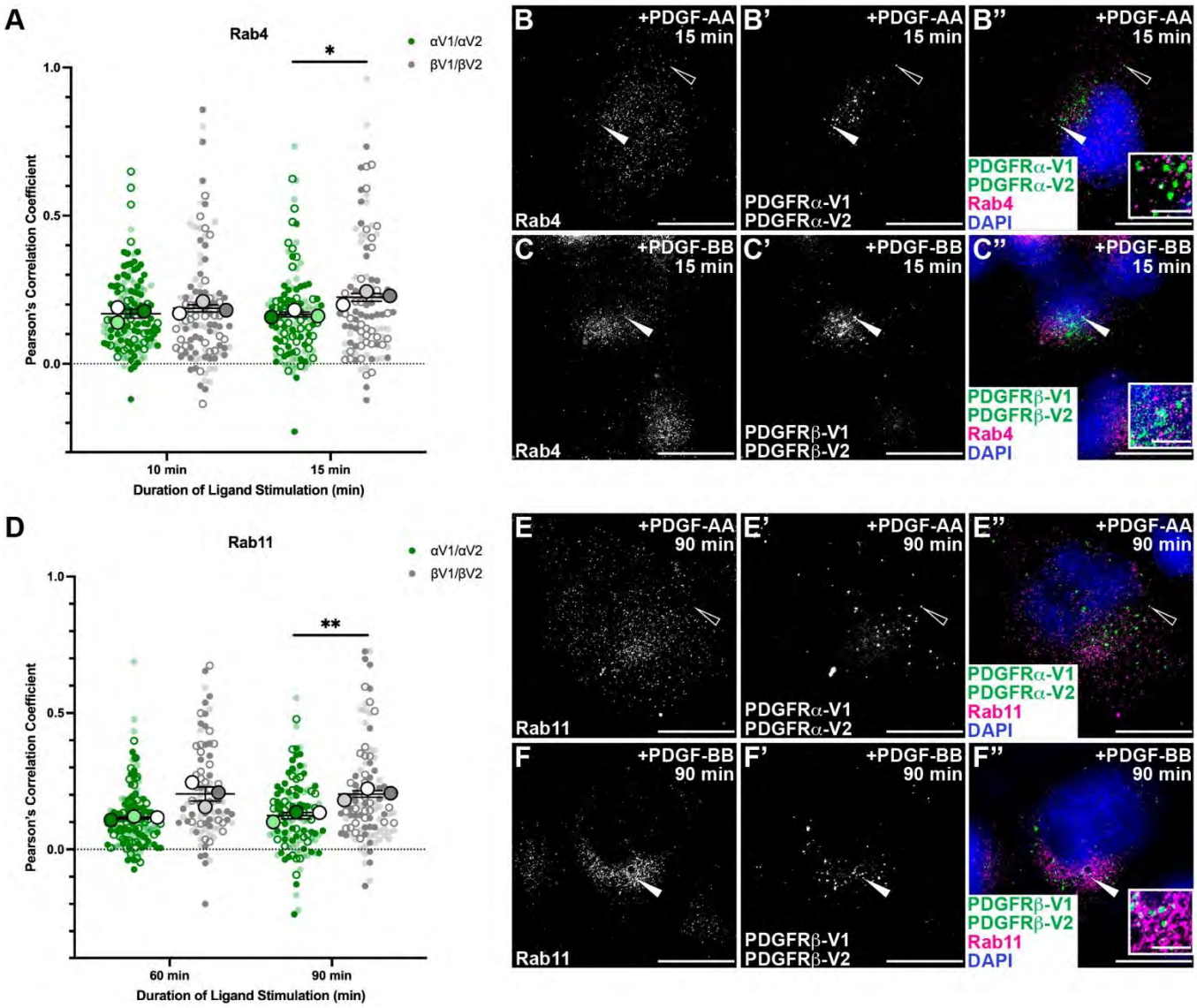

Fig. 5. PDGFRβ homodimers are more likely to be recycled back to the cell membrane than PDGFRα homodimers. (A,D) Scatter dot plots depicting Pearson's correlation coefficient of the PDGFRα homodimer and PDGFRβ homodimer cell lines with an anti-Rab4 antibody (A) or an anti-Rab11 antibody (D) following PDGF ligand stimulation from 10-15 min (A) or 60-90 min (D). Data are mean ± s.e.m. Statistical analyses were performed using a two-tailed, unpaired *t*-test with Welch's correction. *, $p<0.05$; **, $p<0.01$. Colored circles correspond to independent experiments. Summary statistics from biological replicates consisting of independent experiments are superimposed on top of data from all cells. *n*>20 technical replicates across each of 3 biological replicates. (B-C",E-F") Rab4 antibody expression (white/magenta; B,B",C,C") or Rab11 antibody expression (white/magenta; E,E",F,F") and/or Venus expression (white/green; B',B",C',C",E',E",F',F") as assessed by (immuno)fluorescence

analysis of PDGFRα homodimer (B-B”,E-E”) and PDGFRβ homodimer (C-C”,F-F”) cell lines. Insets in B”, C” and F” are regions where white arrows are pointing. Nuclei were stained with DAPI (blue; B”,C”,E”,F”). White arrows denote co-localization; white outlined arrows denote lack of co-localization. Scale bars, 20 μm. Inset scale bars, 3 μm.

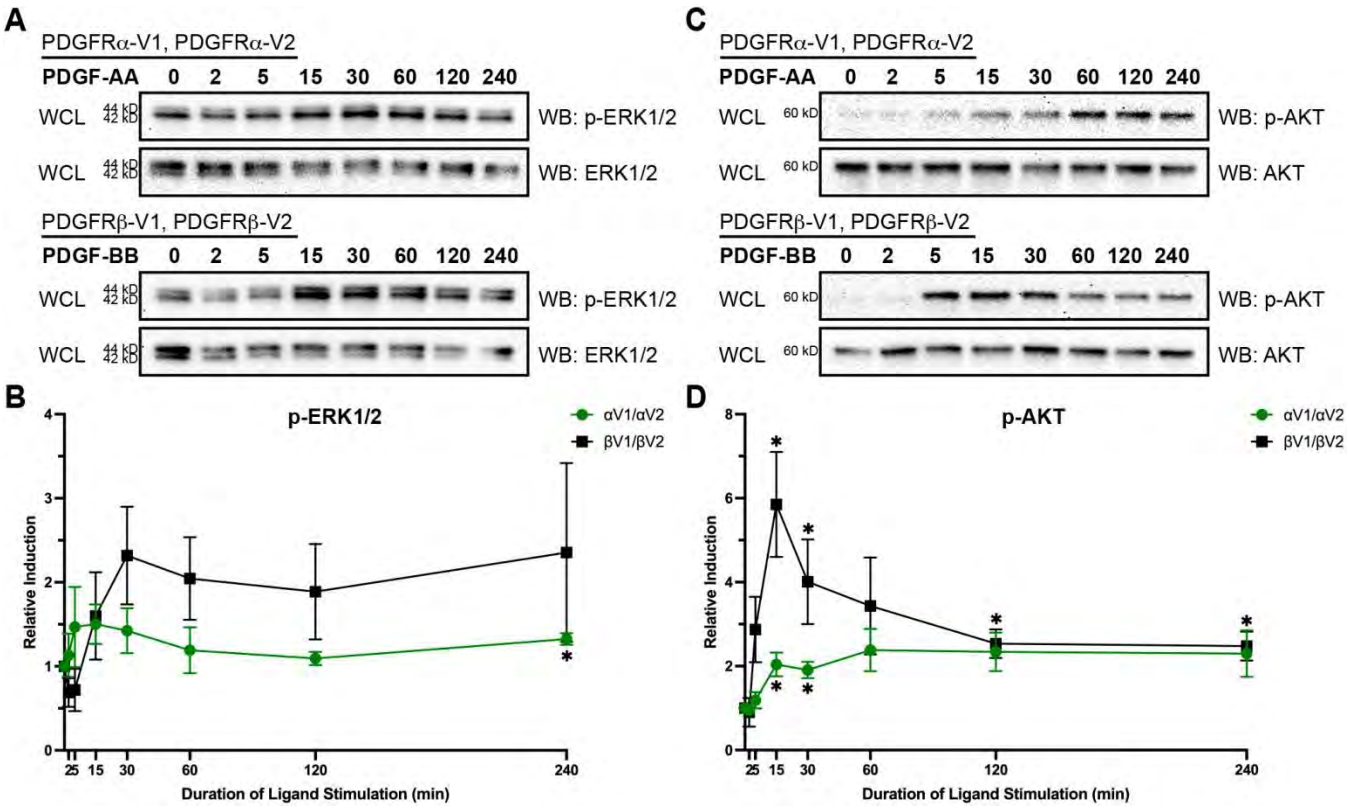

Fig. 6. PDGFRβ homodimer activation induces a greater amplitude of downstream signaling. (A,C) Western blot (WB) analysis of whole cell lysates (WCL) from PDGFRα homodimer (top) and PDGFRβ homodimer (bottom) cell lines following a timecourse of PDGF ligand stimulation from 2 min to 4 h with anti-phospho-ERK1/2 (A) or anti-phospho-AKT (C) antibodies. (B,D) Line graphs depicting quantification of band intensities from $n \geq 3$ biological replicates as in A and C. Data are mean ± s.e.m. Statistical analyses were performed using a two-tailed, ratio paired *t*-test within each cell line and a two-tailed, unpaired *t*-test with Welch's correction between each cell line. *, $p<0.05$.

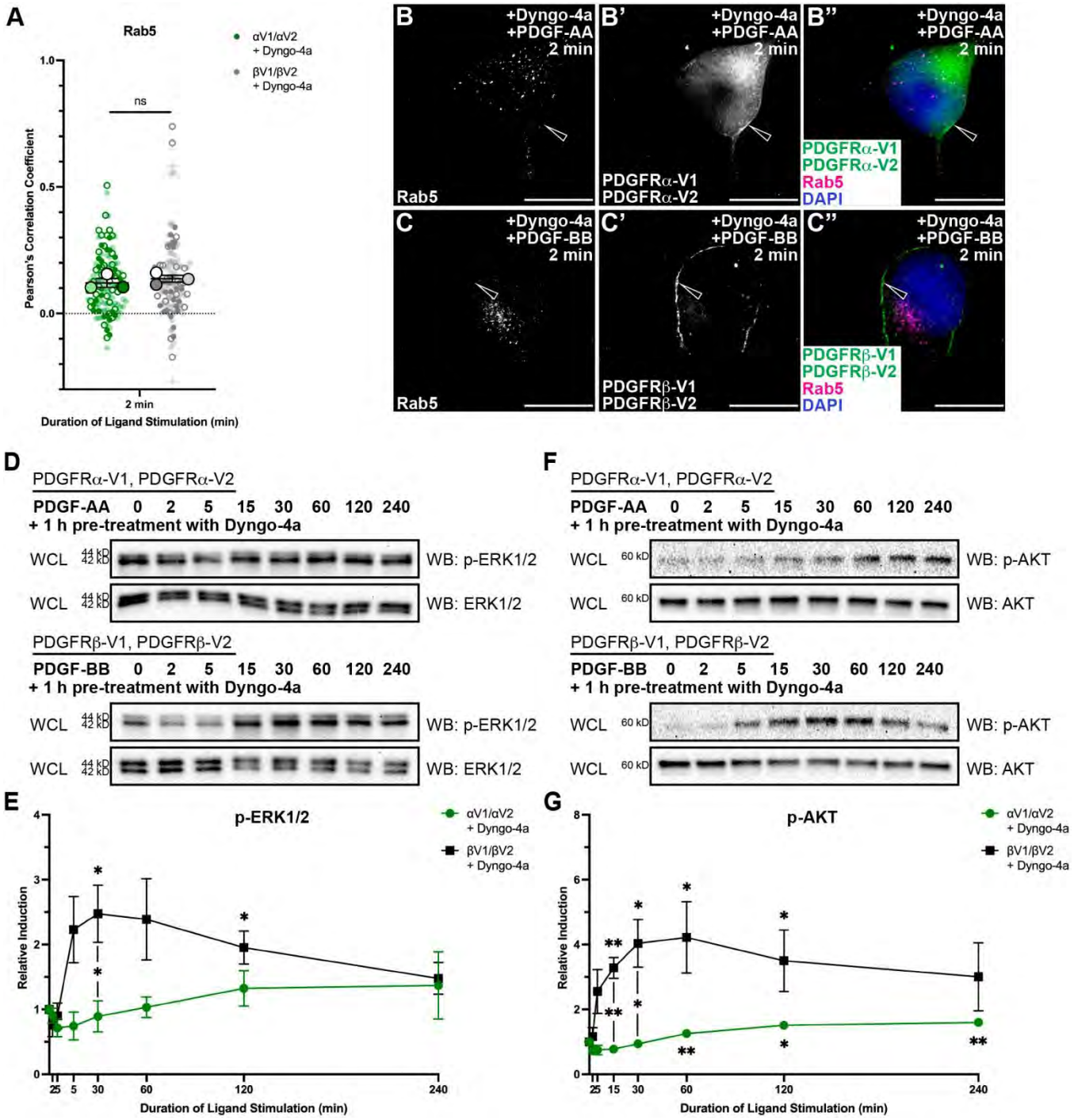

Fig. 7. Inhibition of clathrin-mediated endocytosis results in alterations in cellular trafficking and downstream signaling dynamics, especially for PDGFRα homodimers.

(A) Scatter dot plot depicting Pearson's correlation coefficient of the PDGFRα homodimer and PDGFRβ homodimer cell lines with an anti-Rab5 antibody following pretreatment with 30 μM Dyngo-4a and PDGF ligand stimulation for 2 min. Data are mean ± s.e.m. Statistical analyses were performed using a two-tailed, unpaired *t*-test with Welch's correction between each cell

line. ns, not significant. Colored circles correspond to independent experiments. Summary statistics from biological replicates consisting of independent experiments are superimposed on top of data from all cells. *n*>20 technical replicates across each of 3 biological replicates. (B-C") Rab5 antibody expression (white/magenta; B,B",C,C") and/or Venus expression (white/green; B',B",C',C") as assessed by (immuno)fluorescence analysis of PDGFRα homodimer (B-B") and PDGFRβ homodimer (C-C") cell lines. Nuclei were stained with DAPI (blue; B",C"). White outlined arrows denote lack of co-localization. Scale bars, 20 μm. (D,F) Western blot (WB) analysis of whole cell lysates (WCL) from PDGFRα homodimer (top) and PDGFRβ homodimer (bottom) cell lines following pretreatment with 30 μM Dyngo-4a and a timecourse of PDGF ligand stimulation from 2 min to 4 h with anti-phospho-ERK1/2 (D) or anti-phospho-AKT (F) antibodies. (E,G) Line graphs depicting quantification of band intensities from *n*=3 biological replicates as in D and F. Data are mean ± s.e.m. Statistical analyses were performed using a two-tailed, ratio paired *t*-test within each cell line and a two-tailed, unpaired *t*-test with Welch's correction between each cell line. *, $p<0.05$; **, $p<0.01$.

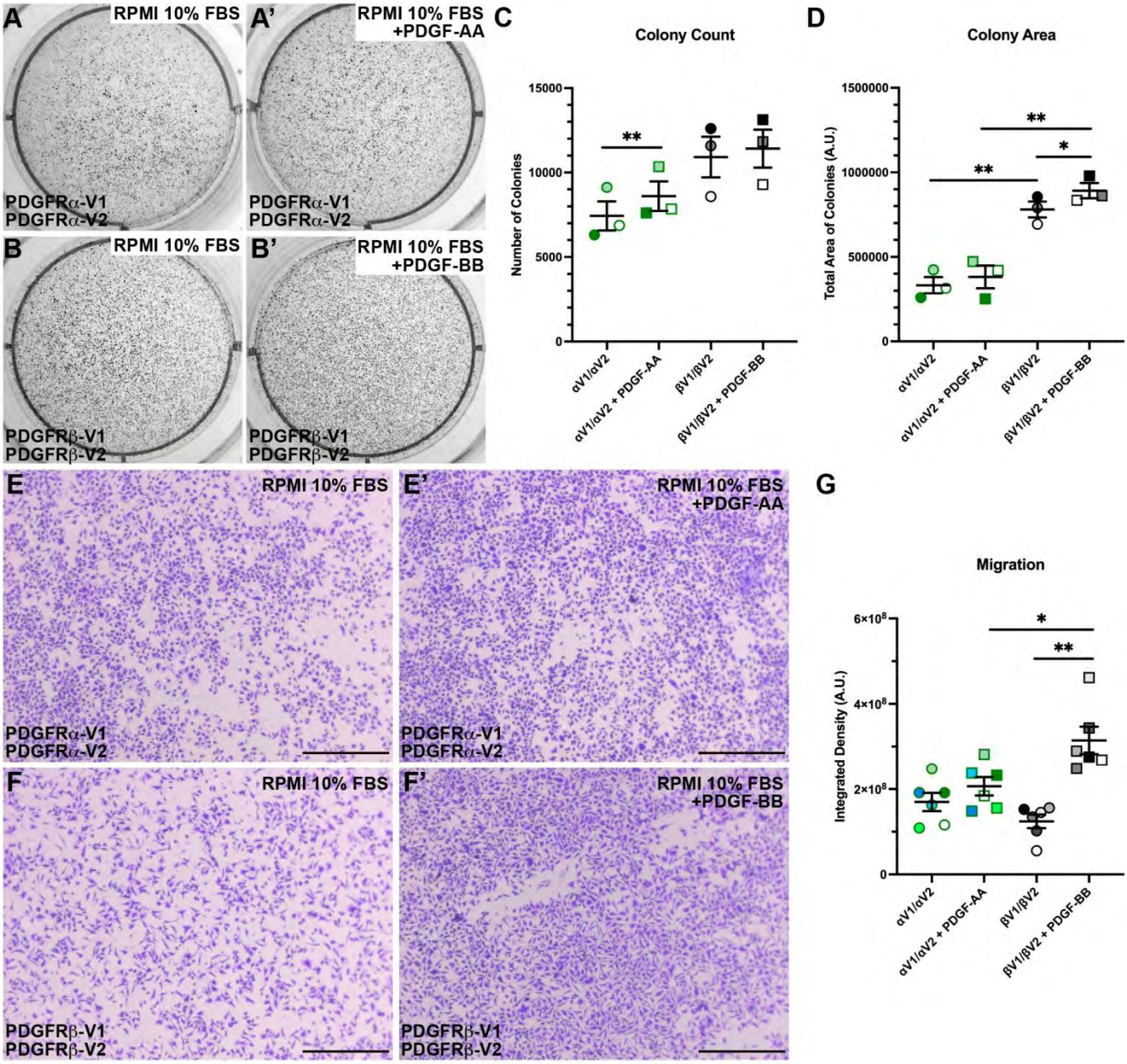

Fig. 8. PDGFRβ homodimer activation leads to greater cellular activity. (A-B') Colony growth in soft agar independent growth assays for PDGFRα homodimer (A,A') and PDGFRβ homodimer (B,B') cell lines after 10 days in RPMI growth medium in the absence (A,B) or presence (A',B') of PDGF ligand. (C,D) Scatter dot plots depicting quantification of colony count (C) or colony area (D) as in A-B'. Data are mean ± s.e.m. Statistical analyses were performed using a paired *t*-test within each cell line and a two-tailed, unpaired *t*-test with Welch's correction between each cell line. *, $p<0.05$; **, $p<0.01$. Colored symbols correspond to independent experiments and represent summary statistics from biological replicates. *n*=2 technical replicates across each of 3 biological replicates. (E-F') Crystal violet staining of

PDGFRα homodimer (E,E') and PDGFRβ homodimer (F,F') cell lines following 24 h of migration through a porous membrane towards RPMI growth medium lacking (E,F) or containing (E',F') PDGF ligand. Scale bars, 50 μm. (G) Scatter dot plot depicting integrated density in arbitrary units (A.U.) as in E-F'. Data are mean ± s.e.m. Statistical analyses were performed using a paired *t*-test within each cell line and a two-tailed, unpaired *t*-test with Welch's correction between each cell line. *, $p<0.05$; **, $p<0.01$. Colored symbols correspond to independent experiments and represent summary statistics from biological replicates. *n*=5 technical replicates across each of 6 biological replicates.

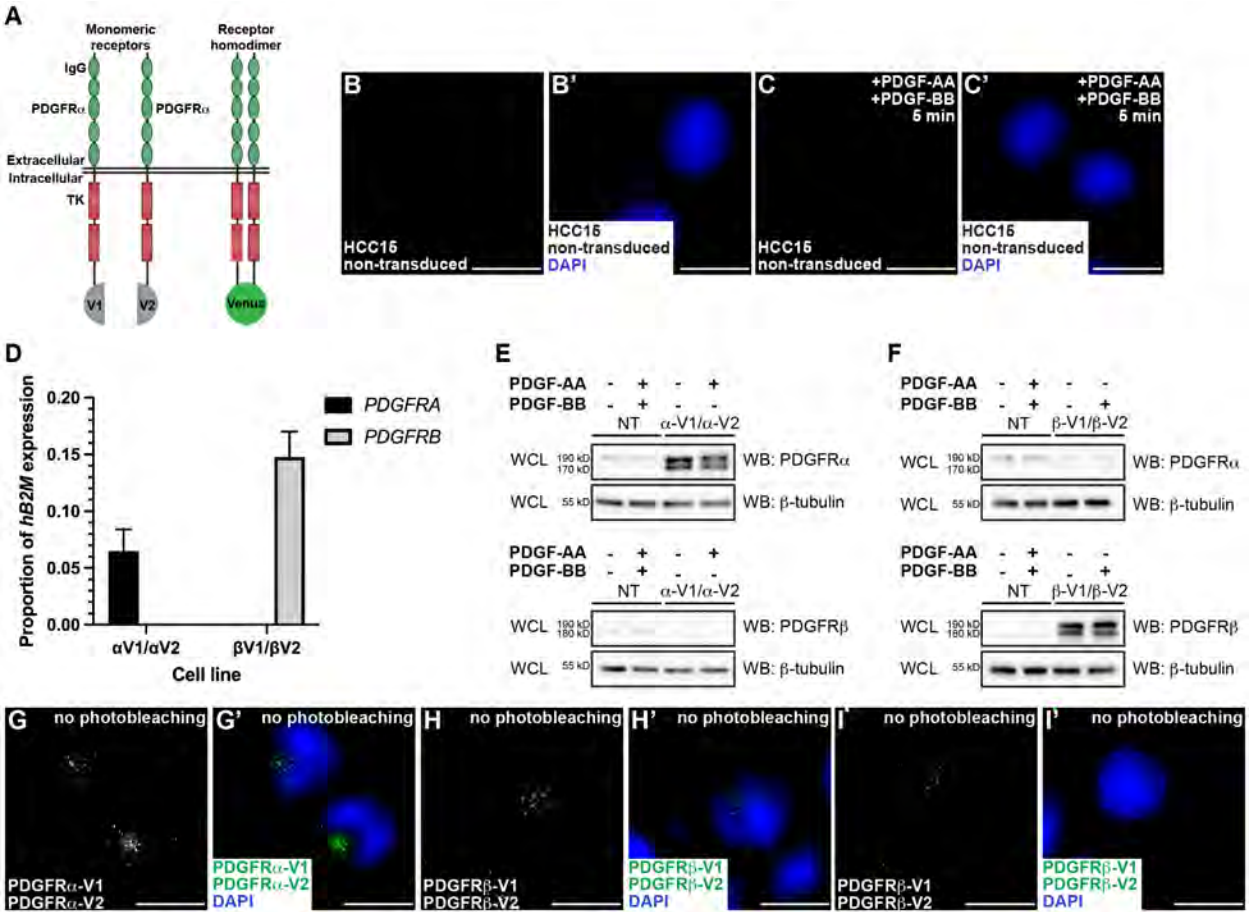

Fig. S1. Validation of PDGFR-BiFC stable cell lines. (A) Schematic of PDGFRα with five extracellular immunoglobulin (IgG) domains and a split intracellular tyrosine kinase (TK) domain fused to the non-fluorescent N-terminal (V1) fragment of Venus and PDGFRα fused to the C-terminal (V2) fragment. Upon receptor dimerization, a functional Venus protein is generated. (B-C') Venus expression (white/green) as assessed by fluorescence analysis of non-transduced HCC15 cells in the absence (B,B') or presence (C,C') of PDGF ligands for 5 min. Nuclei were stained with DAPI (blue; B',C'). Scale bars, 20 μm. *n*>20 technical replicates across each of 3 biological replicates. (D) Bar graph depicting *PDGFRA* and *PDGFRB* expression in PDGFRα homodimer (left) and PDGFRβ homodimer (right) cell lines as assessed by quantitative RT-PCR. Data are mean ± s.e.m. *n*=3 biological replicates. (E,F) Western blot (WB) analysis of whole cell lysates (WCL) from non-transduced (NT) HCC15 cells (left), PDGFRα homodimer (E; right) and PDGFRβ homodimer (F; right) cell lines in the absence or presence of PDGF ligand for 15 min with anti-PDGFRα (top) or anti-

PDGFRβ (bottom) antibodies. *n*=2 biological replicates per condition. (G-I') Venus expression (white/green) as assessed by fluorescence analysis of PDGFRα homodimer (G,G') and PDGFRβ homodimer (H-I') cell lines in the absence of both photobleaching and PDGF ligand stimulation. Nuclei were stained with DAPI (blue; G',H',I'). Scale bars, 20 μm. *n*>20 technical replicates across 1 biological replicate.

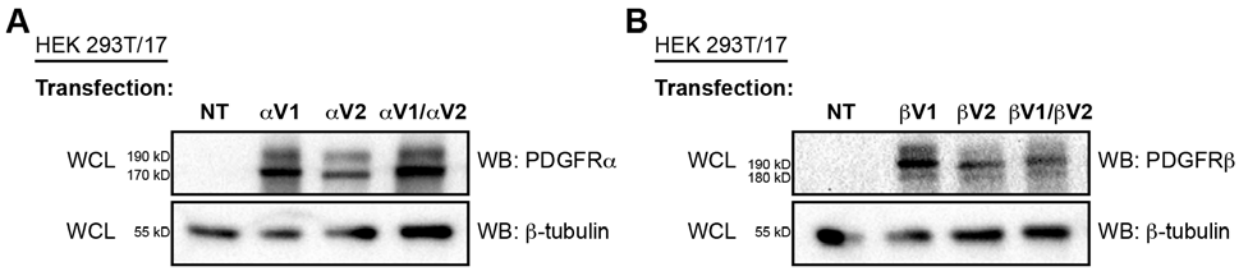

Fig. S2. PDGFR-BiFC constructs express glycosylated and non-glycosylated versions of the PDGFRs. (A,B) Western blot (WB) analysis of whole cell lysates (WCL) from non-transfected (NT) HEK 293T/17 cells and cells transfected with individual PDGFR-BiFC expression constructs as well as relevant combinations of expression constructs with anti-PDGFRα (A) or anti-PDGFRβ (B) antibodies. *n*=1 biological replicate per condition.

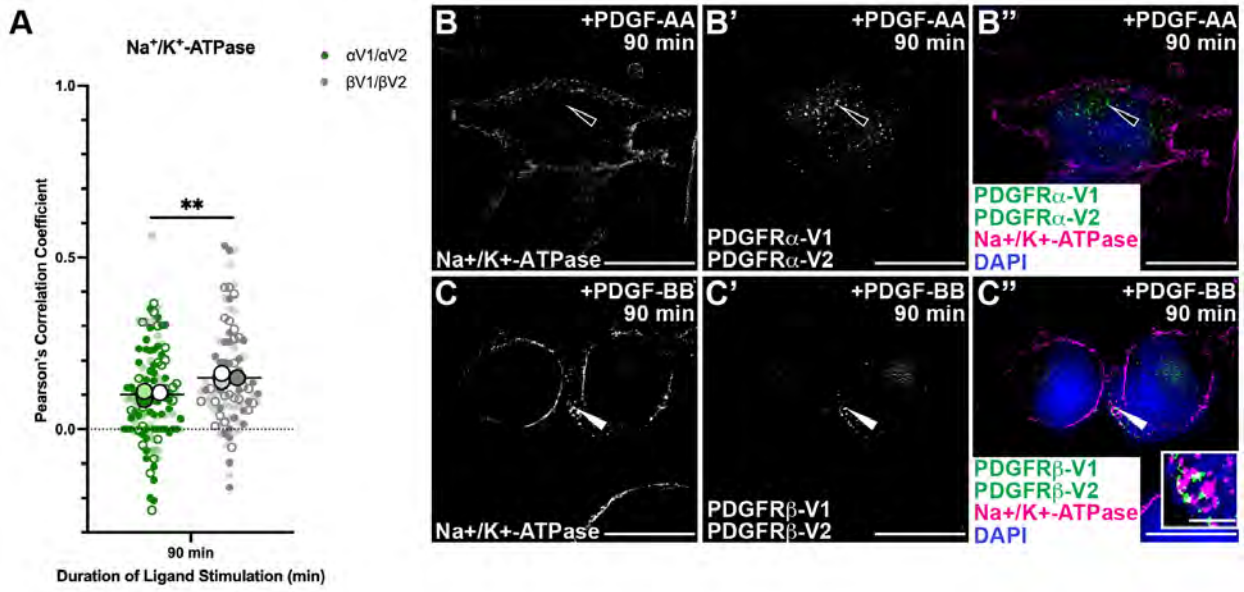

Fig. S3. PDGFRβ homodimers are more likely to localize to the cell membrane following 90 minutes of PDGF ligand stimulation than PDGFRα homodimers. (A) Scatter dot plot depicting Pearson's correlation coefficient of the PDGFRα homodimer and PDGFRβ homodimer cell lines with an anti-Na^+/K^+-ATPase antibody following PDGF ligand stimulation for 90 min. Data are mean ± s.e.m. Statistical analyses were performed using a two-tailed, unpaired *t*-test with Welch's correction. **, $p<0.01$. Colored circles correspond to independent experiments. Summary statistics from biological replicates consisting of independent experiments are superimposed on top of data from all cells. *n*>20 technical replicates across each of 3 biological replicates. (B-C") Na^+/K^+-ATPase antibody expression (white/magenta; B,B",C,C") and/or Venus expression (white/green; B',B",C',C") as assessed by (immuno)fluorescence analysis of PDGFRα homodimer (B-B") and PDGFRβ homodimer (C-C") cell lines. Insets in B" and C" are regions where white arrows are pointing. Nuclei were stained with DAPI (blue; B",C"). White arrows denote co-localization; white outlined arrows denote lack of co-localization. Scale bars, 20 μm. Inset scale bars, 3 μm.

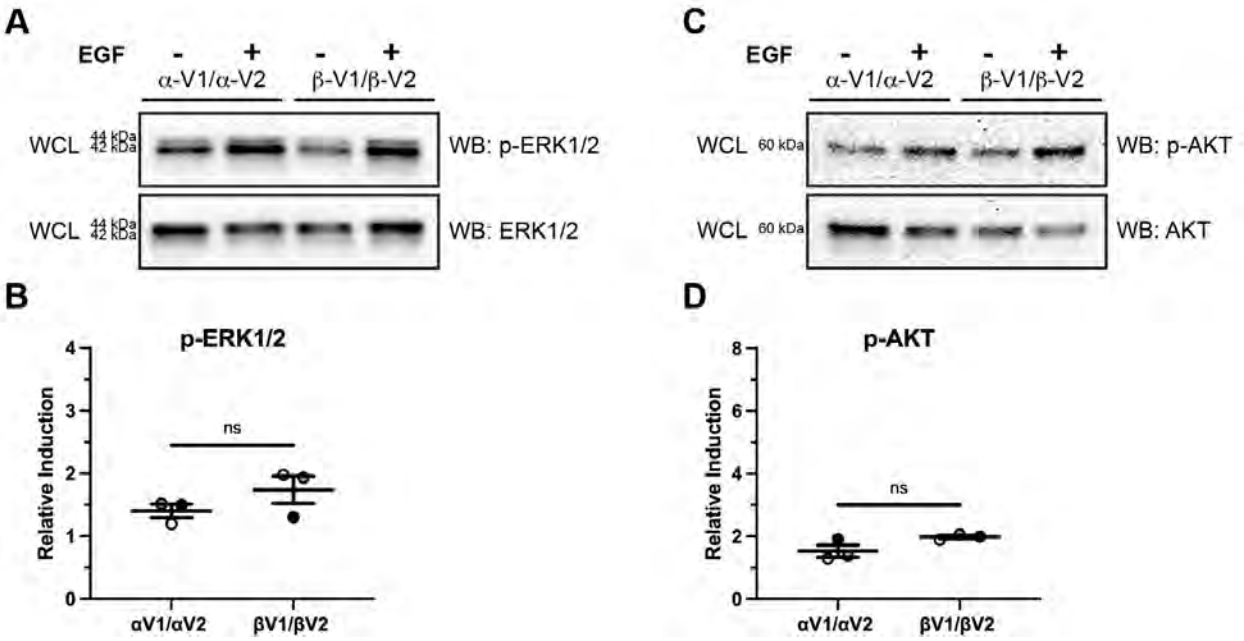

Fig. S4. Phosphorylation of ERK1/2 and AKT downstream of EGF stimulation is unchanged between stable PDGFR-BiFC cell lines. (A,C) Western blot (WB) analysis of whole cell lysates (WCL) from PDGFRα homodimer (left) and PDGFRβ homodimer (right) cell lines in the absence of ligand or following EGF ligand stimulation for 10 min with anti-phospho-ERK1/2 (A) or anti-phospho-AKT (C) antibodies. (B,D) Scatter dot plots depicting quantification of band intensities from *n*=3 biological replicates as in A and C. Data are mean ± s.e.m. Statistical analyses were performed using a two-tailed, unpaired *t*-test with Welch's correction between each cell line. ns, not significant. Shaded circles correspond to independent experiments.

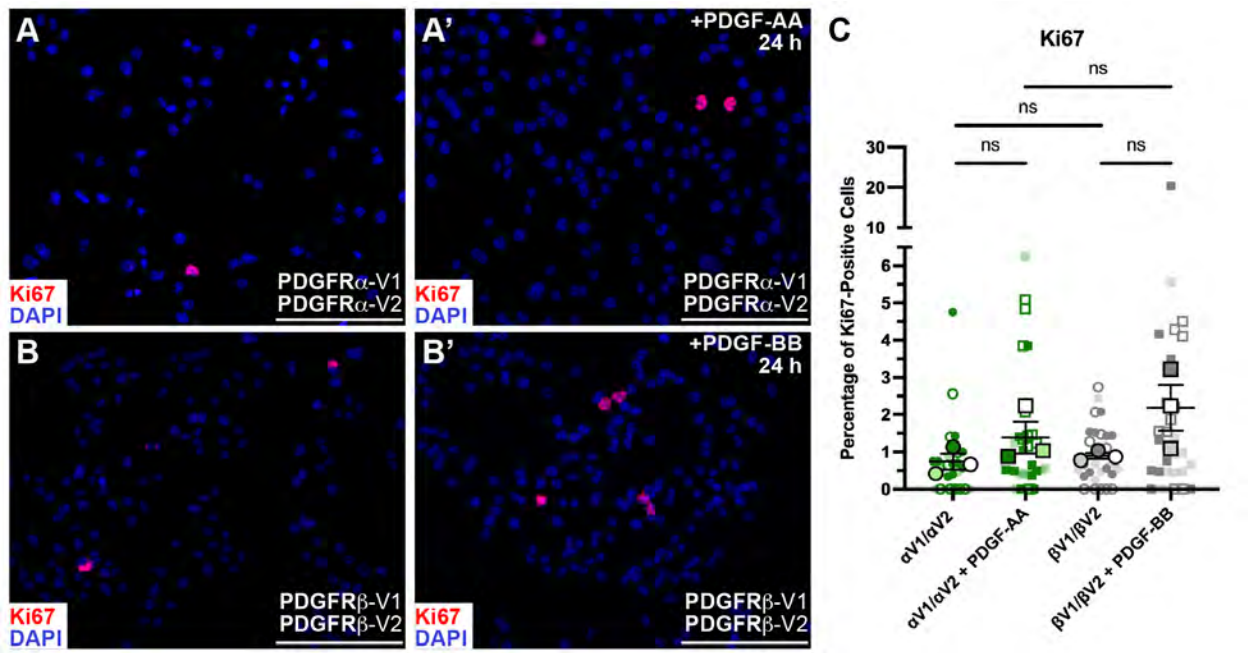

Fig. S5. PDGFRβ homodimer activation leads to increased cell proliferation. (A-B') Ki67 antibody expression (red) as assessed by immunofluorescence analysis of PDGFRα homodimer (A,A') and PDGFRβ homodimer (B,B') cell lines in the absence (A,B) or presence (A',B') of PDGF ligand. Nuclei were stained with DAPI (blue; A-B'). Scare bars, 200 μm. (C) Scatter dot plot depicting percentage of Ki67-positive cells as in A-B'. Data are mean ± s.e.m. Statistical analyses were performed using a two-tailed, paired *t*-test within each cell line and a two-tailed, unpaired *t*-test with Welch's correction between each cell line. ns, not significant. Colored symbols correspond to independent experiments. Summary statistics from biological replicates consisting of independent experiments are superimposed on top of data from all collected fields of view. *n*=10 technical replicates across each of 3 biological replicates.

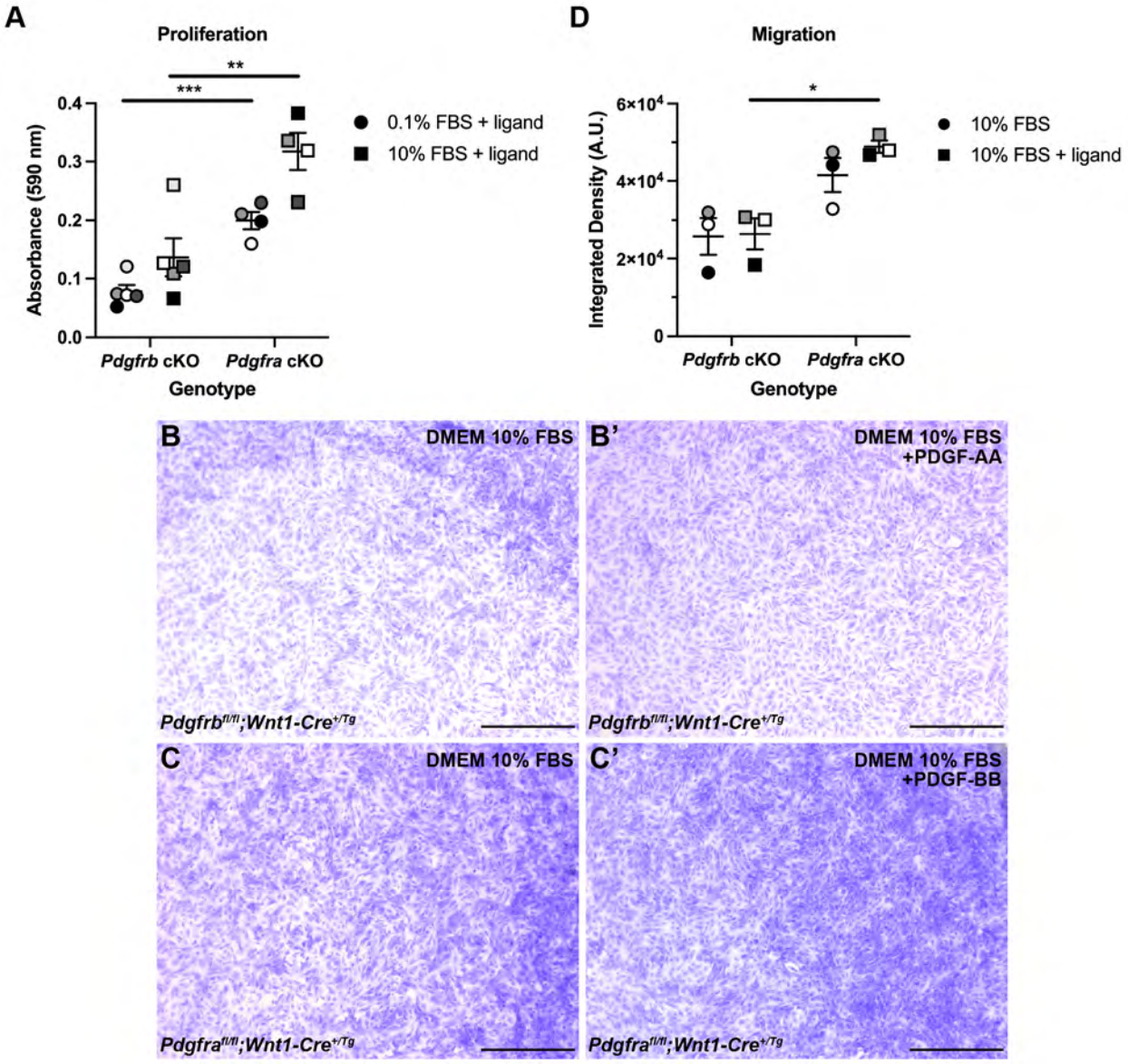

Fig. S6. PDGFRβ homodimer activation leads to greater cellular activity in primary MEPM cells. (A) Scatter dot plot depicting absorbance in crystal violet growth assays for primary MEPM cells expressing PDGFRα (left) or PDGFRβ (right) after 24 h in starvation medium with PDGF ligand or growth medium with PDGF ligand. Data are mean ± s.e.m. Statistical analyses were performed using a two-tailed, unpaired *t*-test with Welch's correction between each cell line. **, p<0.01; ***, p<0.001. Colored symbols correspond to biological replicates across three independent experiments. $n \geq 1$ technical replicates across each of 3 biological replicates. (B-C') Crystal violet staining of cells expressing PDGFRα (B,B') or PDGFRβ (C,C') following 24 h of migration

through a porous membrane towards DMEM growth medium lacking (B,C) or containing (B',C') PDGF ligand. Scale bars, 50 μm. (D) Scatter dot plot depicting integrated density in arbitrary units (A.U.) as in B-C'. Data are mean ± s.e.m. Statistical analyses were performed using a two-tailed, unpaired *t*-test with Welch's correction between each cell line. *, $p<0.05$. Colored symbols correspond to independent experiments and represent summary statistics from biological replicates. *n*=5 technical replicates across each of 3 biological replicates.

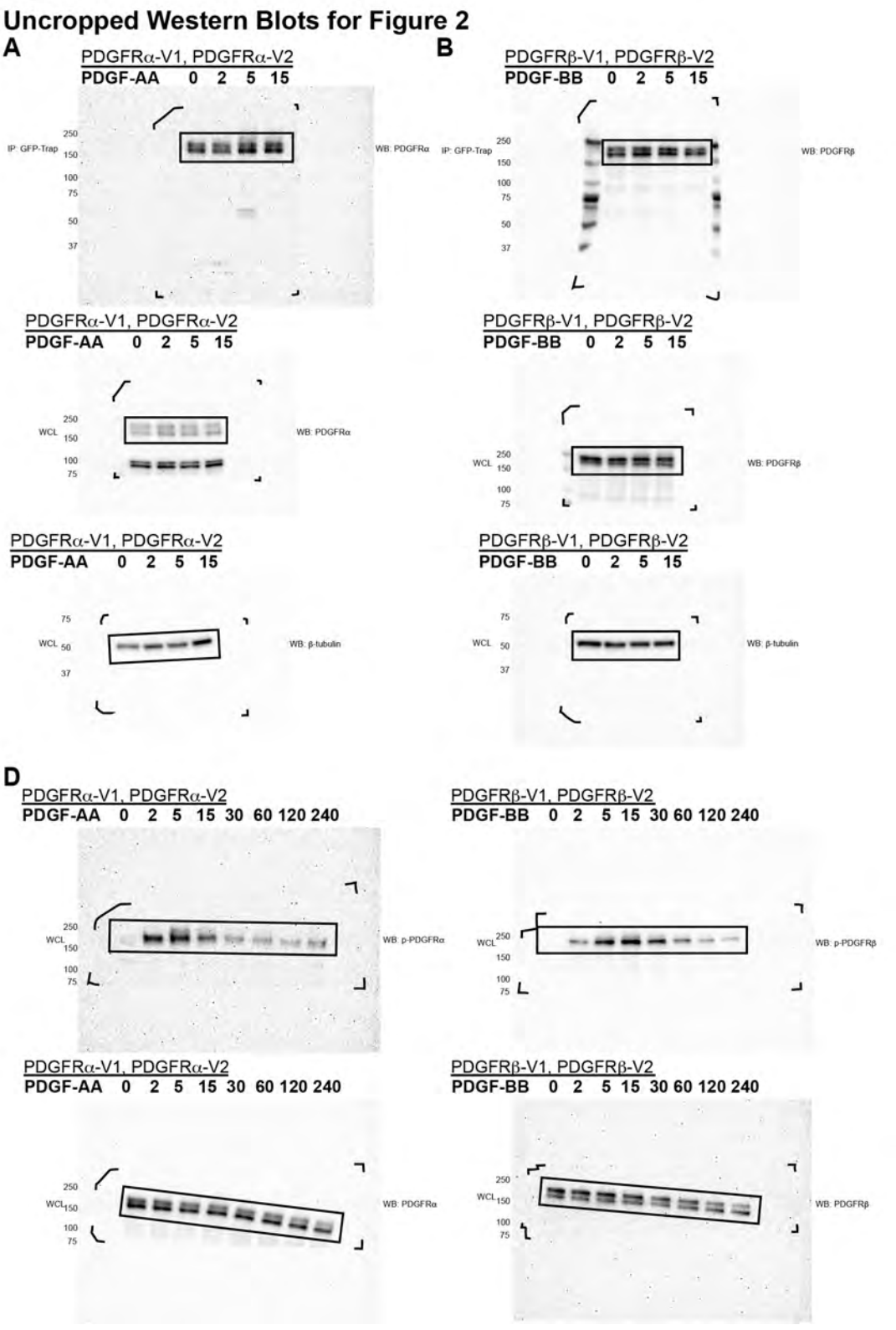

Fig. S7. Full, uncropped western blots. Molecular weight markers are indicated at left and corners of membranes are outlined.

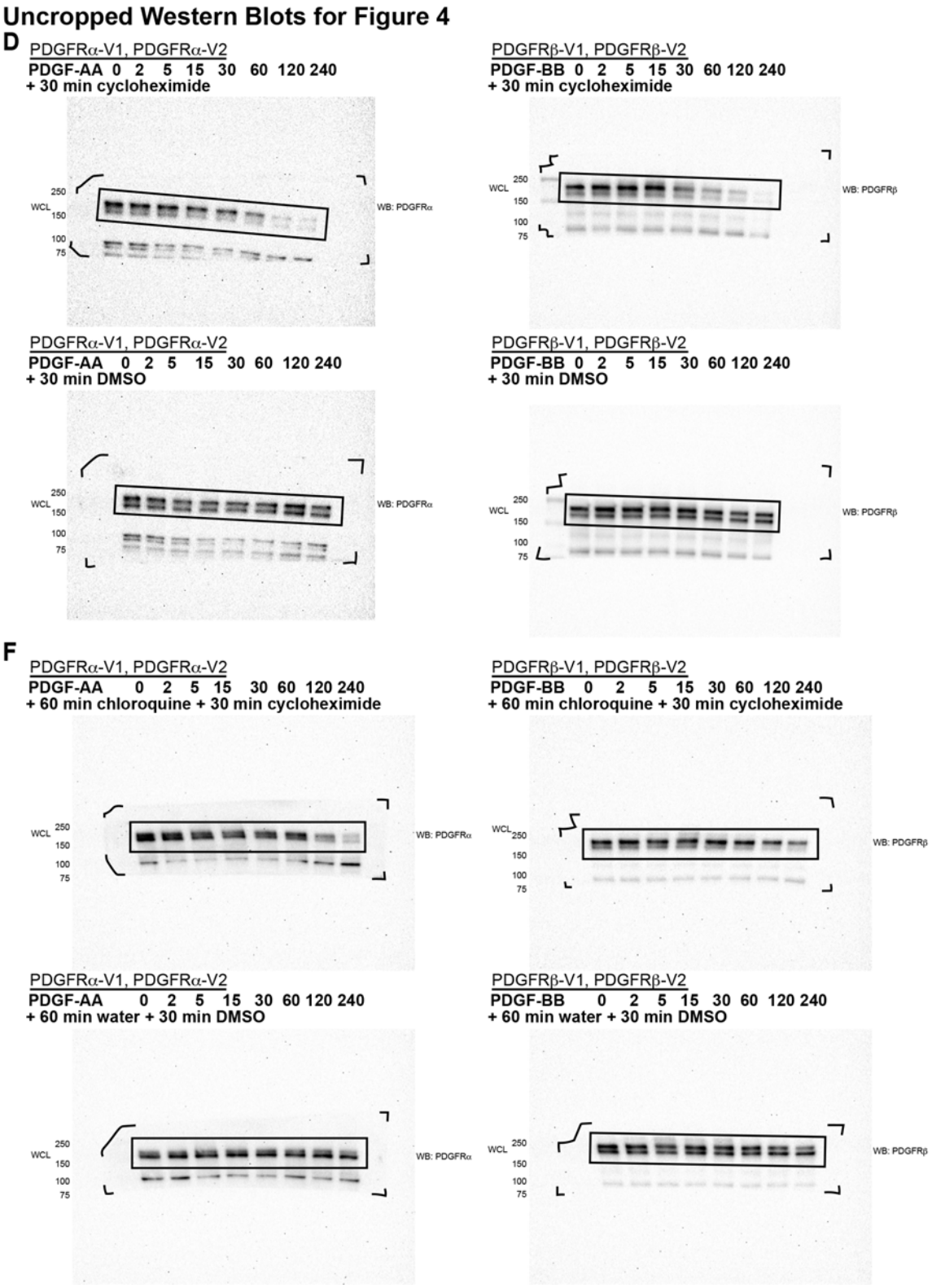

Fig. S8. Full, uncropped western blots. Molecular weight markers are indicated at left and corners of membranes are outlined.

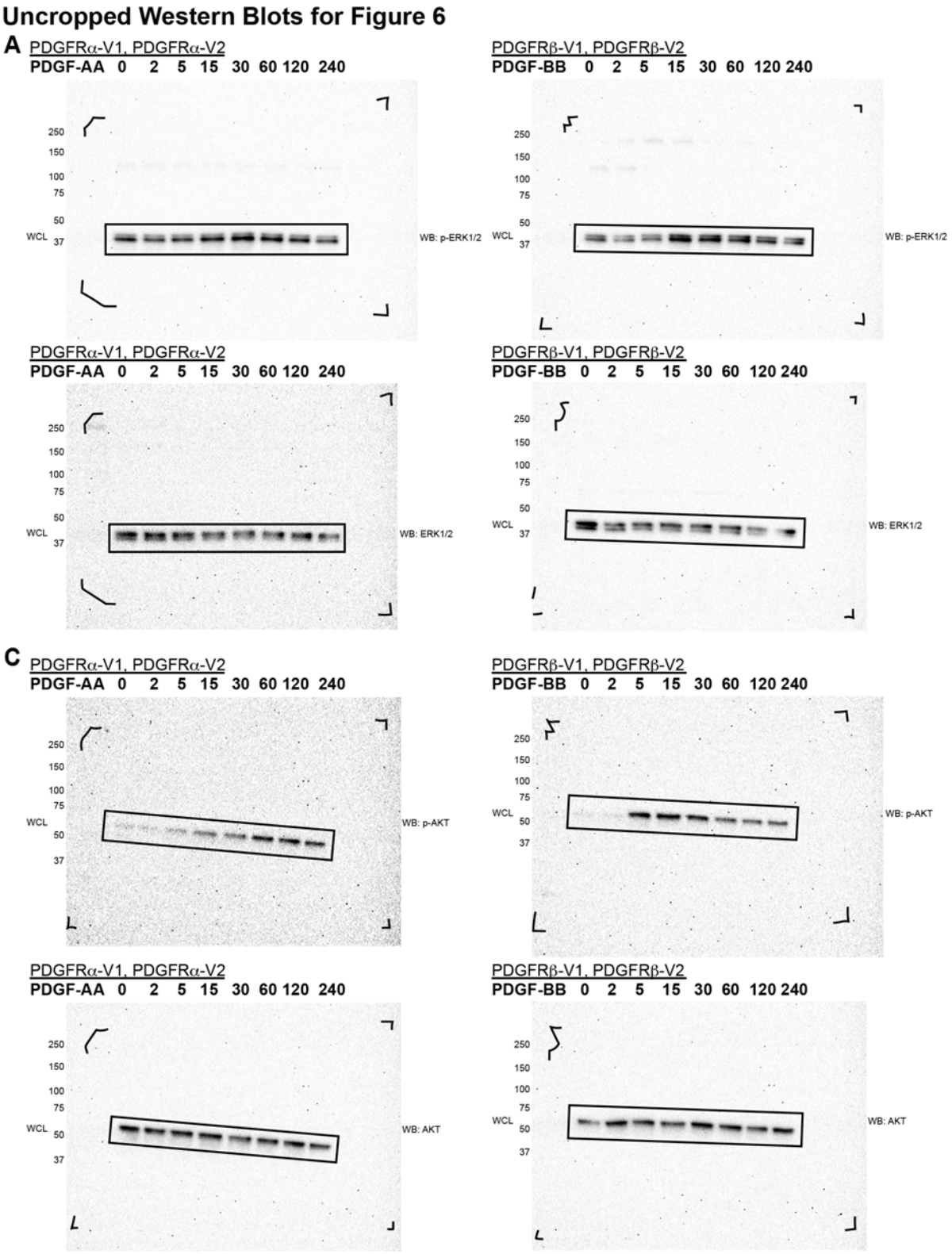

Fig. S9. Full, uncropped western blots. Molecular weight markers are indicated at left and corners of membranes are outlined.

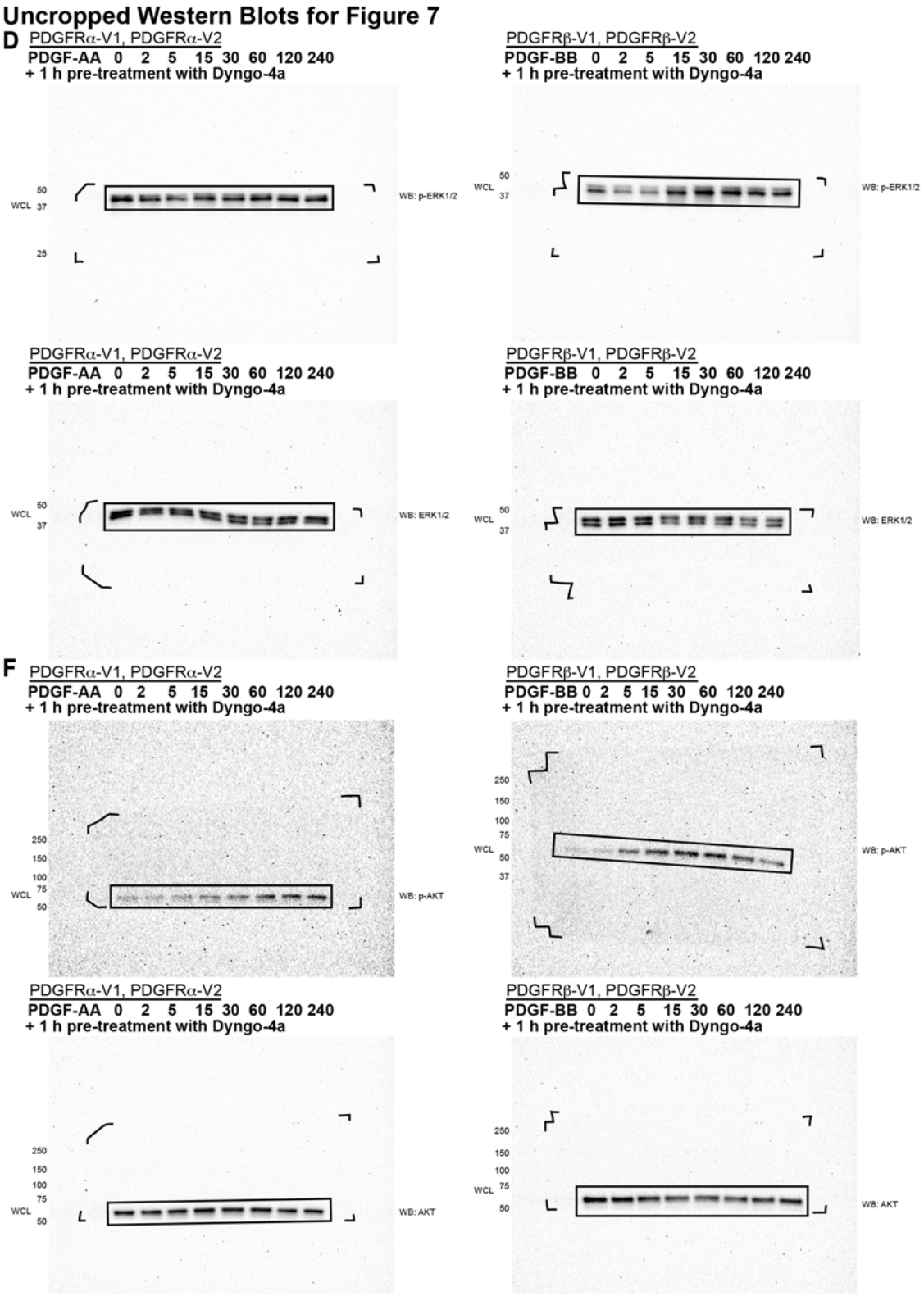

Fig. S10. Full, uncropped western blots. Molecular weight markers are indicated at left and corners of membranes are outlined.

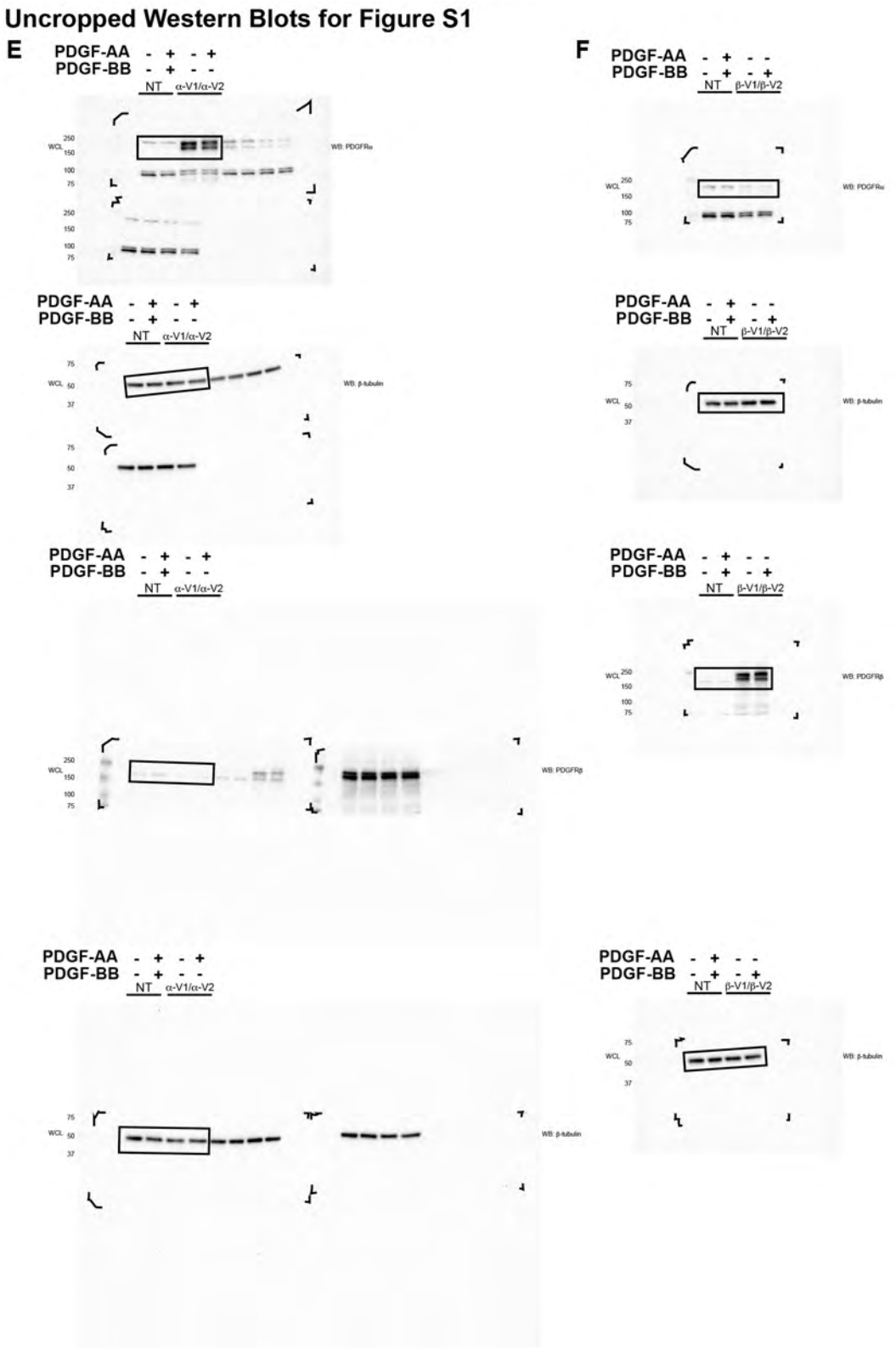

Fig. S11. Full, uncropped western blots. Molecular weight markers are indicated at left and corners of membranes are outlined.

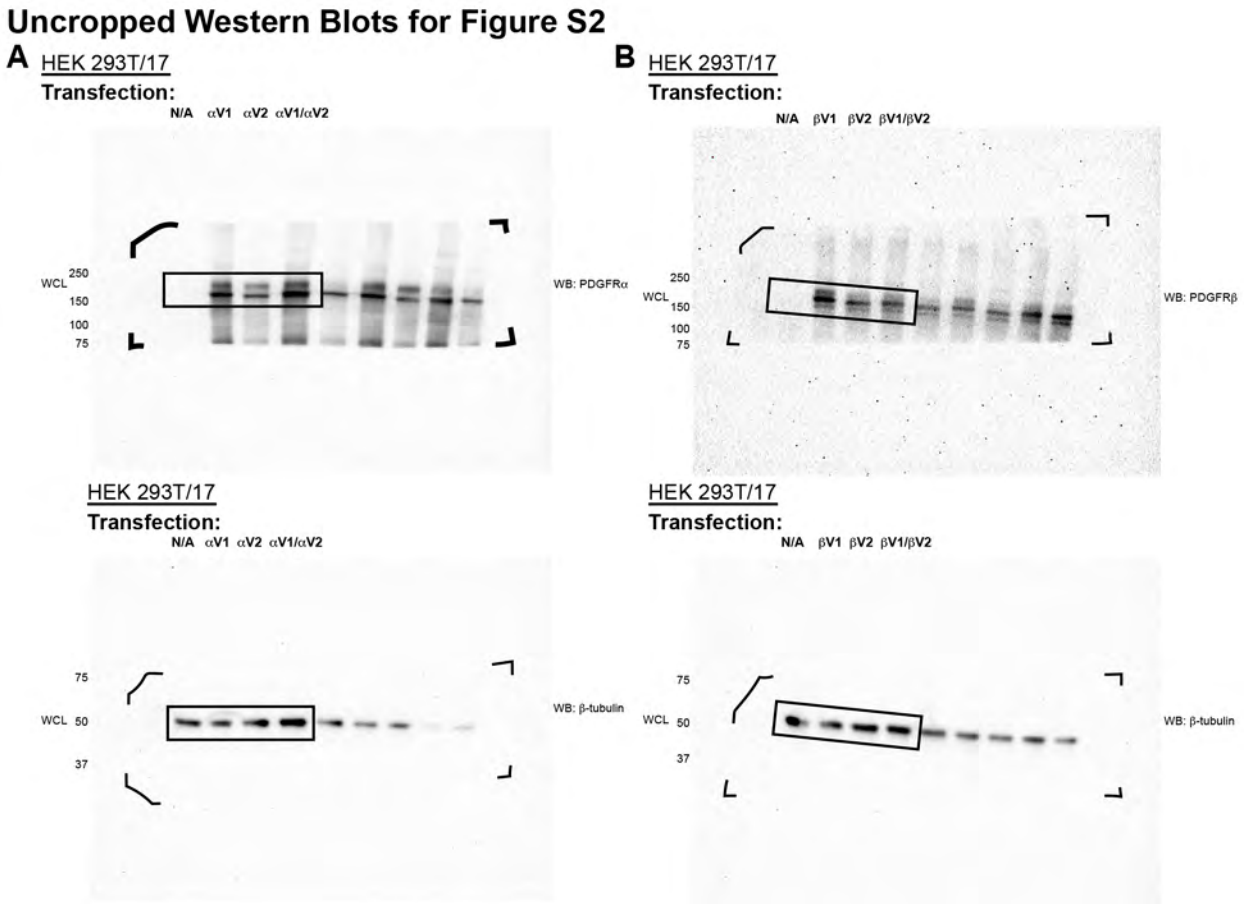

Fig. S12. Full, uncropped western blots. Molecular weight markers are indicated at left and corners of membranes are outlined.

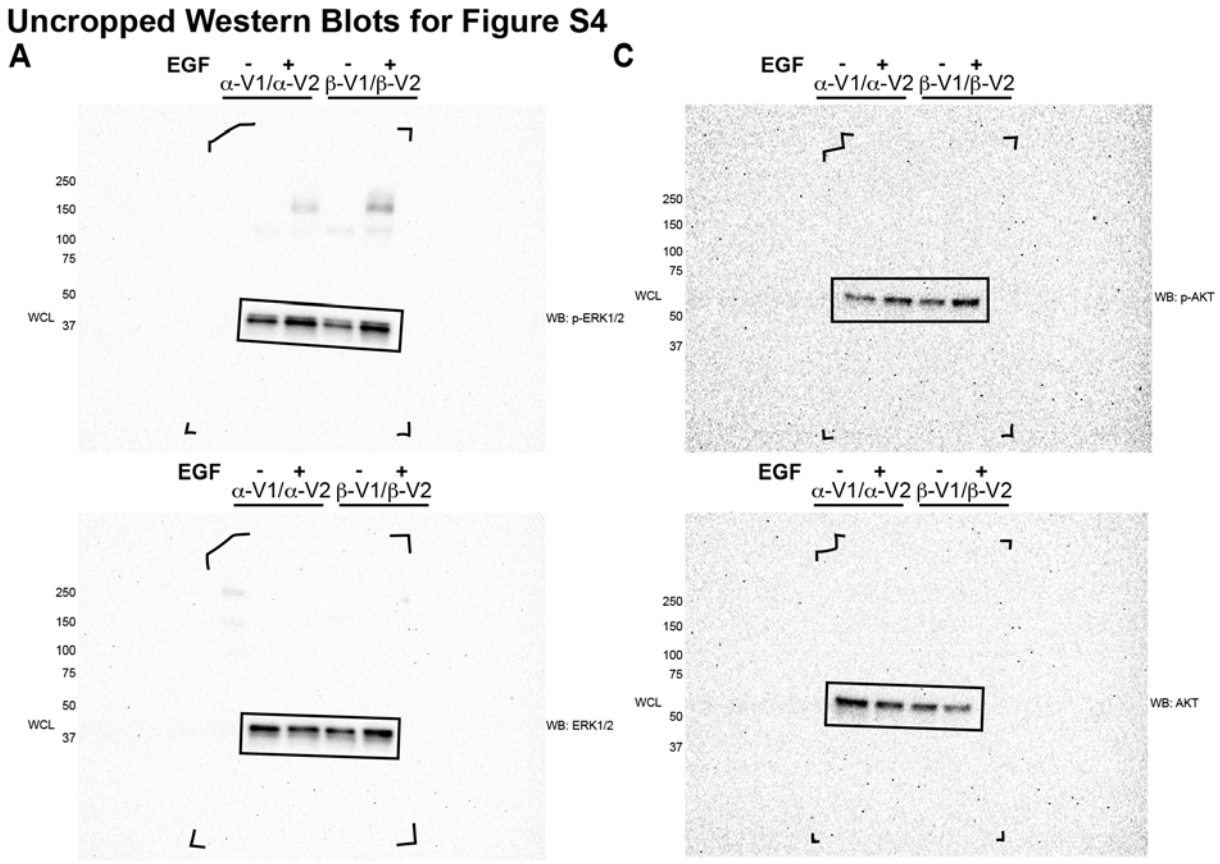

Figure S13. Full, uncropped western blots. Molecular weight markers are indicated at left and corners of membranes are outlined.

Table S1. PCR primers for confirmation of sequence integration.

Common Forward Primer 1	5'-ggagttccgcgttacataac-3'
PDGFRα Reverse 1	5'-GTTGGCCAAAATAGTCCAGG-3'
PDGFRβ Reverse 1	5'- CTGAGATCACCACCACCTTA-3'
PDGFRα Forward 2	5'- GCCGCTTCCTGATATTGAGT-3'
PDGFRα Reverse 2	5'- GAATTATCTAGAGTCGCGGG-3'
PDGFRβ Forward 2	5'- CTGCAGAGACCTCAAAAGGT-3'
PDGFRβ Reverse 2	5'- ccagactgccttgggaaaag-3'

Table S2. PCR primers for qRT-PCR analyses.

B2M Forward	5'-CTACTCTCTCTTTCTGGCCT-3'
B2M Reverse	5'-GACAAGTCTGAATGCTCCAC-3'
PDGFRA Forward	5'-GAAGAGACCCTCCTTTTACC-3'
PDGFRA Reverse	5'-CTTCAGCTTGTCTTCCTCGT-3'
PDGFRB Forward	5'- CAATGCCATCAAACGGGGTT-3'
PDGFRB Reverse	5'- CACTCCTCAGAAACTCCTCA-3'